1

Solar Energy Conversion by Dye-sensitized Photocatalysis

Shunta Nishioka and Kazuhiko Maeda

School of Science, Tokyo Institute of Technology, Department of Chemistry, Tokyo 152-8550, Japan

1.1 Introduction

Dye sensitization enables the generation of charge carriers in a wide-bandgap semiconductor under irradiation by visible light that cannot be absorbed by the semiconductor. Dye-sensitized photocatalysis (DSP) was first proposed by Gerischer in 1972 [1] and was later demonstrated by Grätzel et al. [2]. Because of its potential applications in solar energy conversion, DSP has been studied for decades, especially for H_2 evolution via water splitting [3–5]. The DSP H_2-evolution system consists of two building blocks—a light absorber and a semiconductor material (Figure 1.1)—and the H_2 evolution reaction proceeds as follows: First, the photosensitizer absorbs light and is excited (1). The excited dye injects an electron into a semiconductor (2). The injected electron is consumed via a proton-reduction reaction on the semiconductor's surface, and H_2 is evolved (3). The oxidized light absorber generated by the electron injection returns to the ground state by accepting an electron from a reductant (4). Unfortunately, some undesirable reactions can occur during this reaction scheme (5–7). To improve the overall efficiency of this system, researchers have devoted extensive effort to promoting the forward reactions and impeding the backward reactions.

In this chapter, we present the strategies for improving DSP systems by separating each building block, pointing out the important factors that influence the DSP performance. We survey recent achievements in the DSP field, especially those related to water-splitting systems, including electrochemical systems, and discuss how various factors can be controlled to improve the performance of dye-sensitized systems.

1.2 Light Absorbers

The development of photosensitizers has been rapidly promoted with the growth of the dye-sensitized solar cell (DSSC) field, which has been pioneered by

Water Photo- and Electro-Catalysis: Mechanisms, Materials, Devices, and Systems,
First Edition. Edited by Shaohua Shen and Shuangyin Wang.

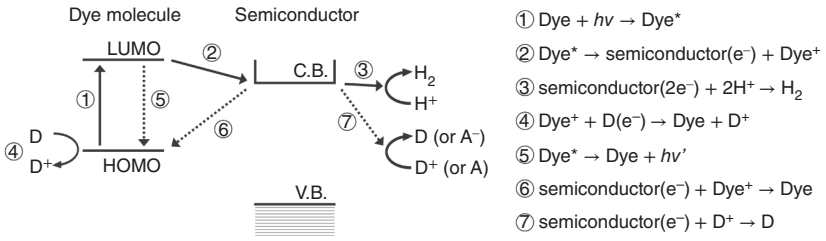

Figure 1.1 Electron transfer processes in a dye-sensitized photocatalysis system. C.B., conduction band; V.B., valence band; HOMO, highest occupied molecular orbital; LUMO, lowest unoccupied molecular orbital; D, electron donor; D^+: oxidized electron donor; A, electron acceptor; A^-, reduced electron acceptor. Solid and broken arrows represent forward and backward electron transfers, respectively.

Tsubomura and coworkers [6] and by O'Regan and Grätzel [7]. The practical application of dye-sensitized photovoltaic cells became realistic with the development of a trinuclear Ru complex that possesses two cyano-bridges and four carboxyl-anchoring groups (Figure 1.2a) [8]. A substantial achievement in the DSSC field is the exploitation of the **N3** dye (Figure 1.2b); the electron-injection quantum yield (QY) from **N3** into TiO_2 has reached almost unity, with a solar-to-electric conversion efficiency of 10% under AM1.5G illumination [9]. The structure of **N3** is very similar to the anchoring unit of the trinuclear dye in that **N3** has four carboxyl-anchoring moieties and two isothiocyanato ligands. The next excellent dye developed was **N719** (Figure 1.2c), which gave a power conversion efficiency greater than 9.18% under AM1.5G. This value is still high even now, although the original work was published 20 years ago [10, 11]. These highly efficient dyes for DSSCs, however, have not been well utilized in DSP systems because of the difference in the DSSC and DSP catalytic cycles. In the case of DSSCs, the injected electrons in a semiconductor (e.g. TiO_2) should migrate quickly to reach the counter electrode through an external circuit. Because of the rapid collection of the injected electrons, acceleration of the electron-injection process by strong coupling between the dye and the semiconductor is effective for DSSC systems. In the case of DSP, however, a surface catalytic reaction involving multi-electron transfer (e.g. proton reduction) would become the rate-determining step, whose time scale is at least four orders of magnitude slower than that of the excited-charge-carrier transfer processes [5]. This is distinct from DSSCs, which are operated by single electron transfer processes. Accelerating the electron injection leads to an increase in the standby electrons in the conduction band for the catalytic reaction, which is not effective for DSP systems. On the contrary, the strong coupling may promote undesirable back electron transfer from the conductive substrate to the oxidized dye [12]. Therefore, the dyes developed for DSSCs need to be modified for use in DSP systems. In this section, new dyes developed for efficient DSSCs are introduced and then dye sensitizers optimized for DSP are discussed.

Before moving to the details, we here explain the basic molecular design of photosensitizers. One of the most studied classes of dyes is metal complexes, which have been used in pioneering research in DSP systems [2, 3, 5] and DSSCs

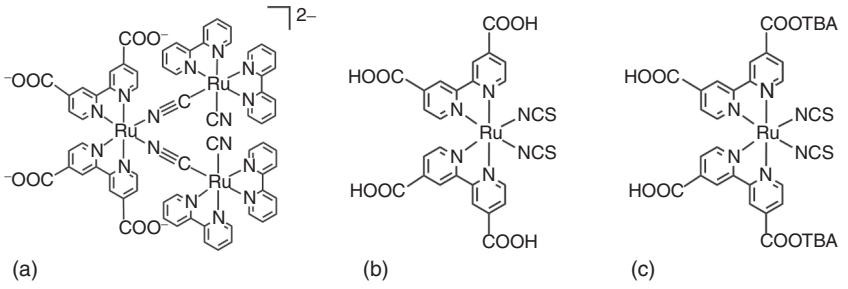

Figure 1.2 Molecular structures of (a) $[Ru(bpy)_2(CN)_2]_2Ru(bpy(COO)_2)_2^{2-}$ (bpy = 2,2′-bipyridine), (b) **N3**, and (c) **N719**. TBA: tetrabutylammonium.

[4, 7–11]. Recent advances in the DSP for H_2 evolution have included the development of Ru [13], Zn [14], and Ir [15] complexes, and these complexes are still mainstream materials used in the DSP field because their photo- and physicochemical properties are chemically controllable. Visible-light absorption by metal complexes used in dye-sensitized systems originates mainly from metal-to-ligand charge transfer (MLCT). The highest occupied molecular orbital (HOMO) and the lowest unoccupied molecular orbital (LUMO) are distributed around the metal center and the ligands, respectively. There are three important properties for an effective sensitizer: (i) wide and strong absorption in the visible region, (ii) an efficient excited-charge-carrier transfer cycle, and (iii) high stability. Shifting the HOMO and LUMO levels varies the light-absorption properties of dyes. Efficient excited-charge-carrier transfer is achieved through vectorial electron transfer. Increased stability is attained via strong adsorption onto a semiconductor.

All three of the aforementioned important properties for designed dye molecules can be achieved through adaptation of the ligands of the metal complex. A tris(bipyridine)ruthenium(II) derivative is a good example for explaining the molecular design of metal complexes (Figure 1.3a). For a dye to adsorb onto a semiconductor, at least one of the bipyridine ligands should be functionalized with an anchoring moiety, which should be located at the position closest to the semiconductor substrate. In such a case, the LUMO of the complex is distributed at the functionalized bipyridine ligand, which enhances electron injection from the excited-state complex into the semiconductor. Therefore, if the other peripheral ligand(s) possess a higher energy than the anchoring ligand, the excited electrons would gather on the anchoring ligand, thereby accelerating the electron injection. In addition, because the electron density of the metal center should be increased to ensure wide visible-light absorption, the peripheral ligand(s) should demonstrate electron-donating behavior. Triphenylamine, which exhibits strong electron-donating ability, was introduced onto a Ru complex as a secondary electron donor unit [16]. Although a triphenylamine-based dye had been studied previously [17], excellent dyes that possess a triphenylamine moiety as an electron donor were developed in the same period [18–20]. The triphenylamine-based dyes have a donor–π–acceptor (D–π–A) conjugated structure, which consists of carbon–carbon double-bonded π-bridges and a cyano electron-acceptor group

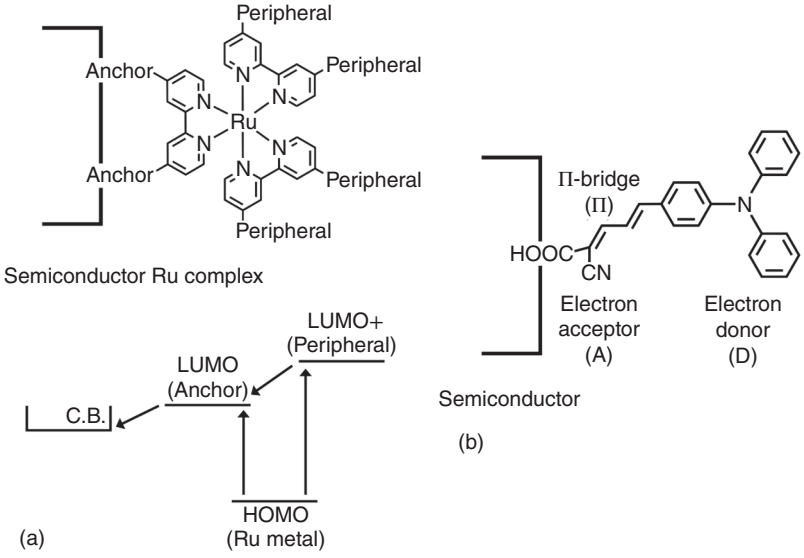

Figure 1.3 Structures of (a) a Ru trisdiimine complex and (b) a triphenylamine-based organic sensitizer. The bottom of figure (a) shows a schematic of the electron-transfer processes of a Ru complex–semiconductor hybrid material. LUMO+: an unoccupied molecular orbital with an energy level higher than that of the LUMO.

(Figure 1.3b). The D–π–A structure enables vectorial charge transfer, which is one of the aforementioned important characteristics of dye-sensitized systems. One of the triphenylamine-based dyes gave an overall **DSSC** efficiency of 5.3%, which is similar to the efficiency of N719 (7.7%). This advancement triggered the rapid development of organic dyes, which are now also used for DSP H_2 evolution. DSP for H_2 evolution has been studied using triphenylamine [21, 22], an organoboron complex [23], coumarin [24], perylene [25], calixarene [26], and tetrathiafulvalene [27], as building blocks for photosensitizers. During the development of these photosensitizers, numerous factors for improving dye-sensitized systems have been revealed. We here discuss these factors, along with some examples of dyes demonstrating the effect of each factor.

1.2.1 Extending the Light Absorption Spectra of Dyes

Extending the absorption spectrum of a dye is a common approach to efficiently utilizing sunlight for solar energy conversion. The strategy for extending the absorption of a dye appears simple: shift the LUMO downward and/or the HOMO upward. The reality, however, is not straightforward because two requirements must be met [28]. First, an excited-state dye must inject an electron into the semiconductor. Second, a sensitizer needs to oxidize a reductant or electron mediator to regenerate the ground state. Extensive efforts have been devoted to developing new photosensitizers that enable the more efficient utilization of solar energy while still achieving these two requirements.

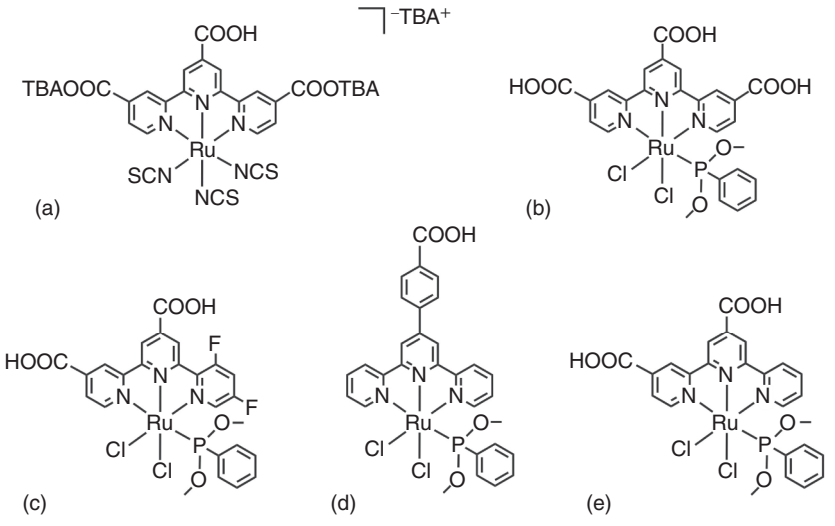

Figure 1.4 Molecular structures of the (a) **N749**, (b) **DX1**, (c) **GS11**, (d) **GS12**, and (e) **GS13** dyes.

Grätzel's group synthesized a panchromatic dye (black dye), **N749** (Figure 1.4a), using a tridentate terpyridine derivative ligand and three thiocyanato ligands [28]. The development of such a panchromatic dye is the ideal approach under the conventional strategy. The absorption spectrum of the sensitizer was extended by the introduction of three thiocyanato ligands that shift the ruthenium(II) t_{2g} orbitals upward. The LUMO level was kept at a more negative potential than the conduction band of TiO_2, and the HOMO was located at a sufficiently positive potential relative to the redox potential of the reductant (i.e. iodide). Recently, Segawa and coworkers developed a phosphine-coordinated Ru-complex sensitizer, **DX1** (Figure 1.4b) [29]. Their approach to extending the absorption of the dye is unconventional in that it involves a spin-forbidden transition. Figure 1.5a shows the absorption and emission spectra as functions of the energy diagrams of **DX1**, along with the spectrum of a black dye. In the case of **DX1**, the singlet–triplet transition is emphasized clearly, and this extension of the light-absorption spectrum improved the power conversion efficiency in a DSSC system.

DX1 and its derivatives have been investigated in a DSP for H_2 evolution [13]. Four phosphine-coordinated Ru complexes (Figure 1.4b–e) were synthesized; their energy diagrams are shown in Figure 1.5b. In all cases, the LUMO level was sufficiently negative for excited-electron injection into the conduction band of TiO_2. These four panchromatic photosensitizers were applied to the photocatalytic H_2-evolution reaction on Pt-modified TiO_2, where triethanolamine (TEOA) was used as a sacrificial electron donor. **GS12** showed the highest H_2-evolution activity, and the apparent quantum yield (AQY) for H_2 evolution under irradiation by a 400 W Hg lamp reached 5.16%. This value is 5.5 times greater than that of **N719** under the same conditions. The activity increased in the order **GS12** > **GS11** > **DX1** > **GS13**, and this trend obviously reflects the LUMO energy level. These results indicate that

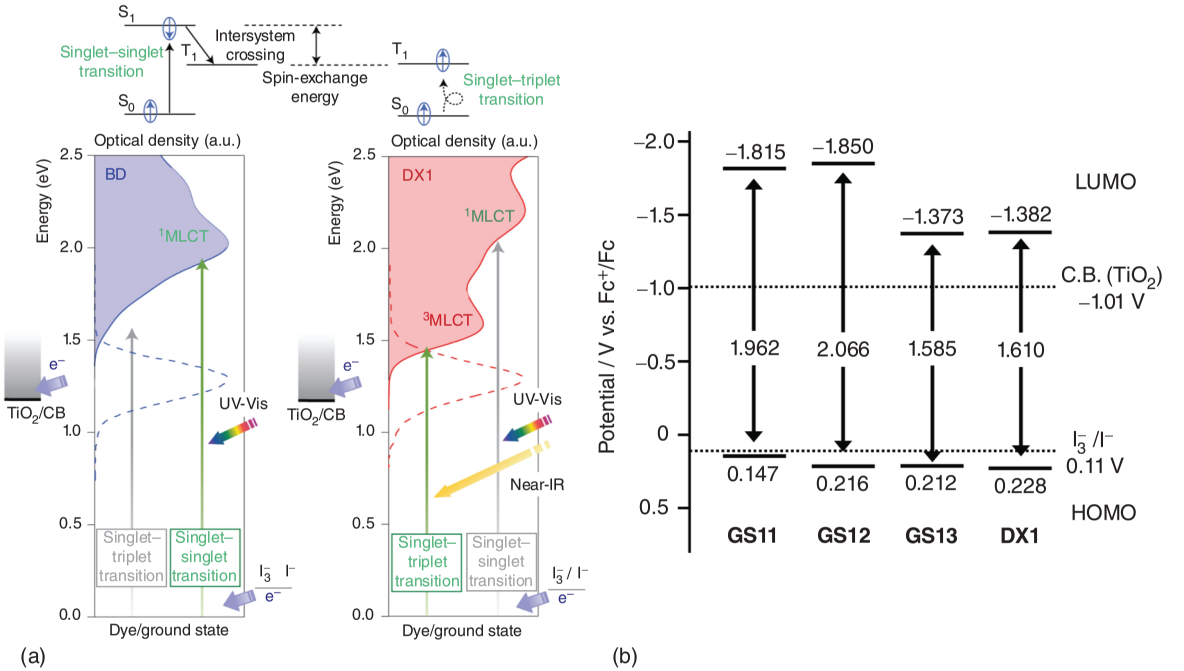

Figure 1.5 (a) Energy diagram of the components and the device performance of the sensitizers. Absorption (solid line) and emission (dashed line) spectra vs. the energy diagrams of BD (black dye, **N749**, left) and **DX1** (right). In the singlet-to-singlet transition, the electron transition from the S_0 to the T_1 excited states causes energy loss via spin-exchange energy (top). Source: Reproduced with permission from Kinoshita et al. [29]; © 2013, Springer Nature. (b) Schematic energy levels of **GS11**, **GS12**, **GS13**, and **DX1**. Source: Adapted with permission from Swetha et al. [13]; © 2015, American Chemical Society.

the DSP performance for the H_2-evolution reaction can be enhanced by negatively shifting the oxidation potential of the dye in the excited state. The use of a panchromatic dye in a dye-sensitized H_2-evolution system improved the photocatalytic activity, and an investigation of the **DX1** derivatives revealed that regulation of the LUMO energy level is an important consideration in the molecular design of sensitizers.

1.2.2 Enhancement of the Absorption Coefficient of Dyes

Increasing the molar extinction coefficient of dyes is a straightforward method of increasing the solar energy conversion efficiency in a dye-sensitization system. Making the π-chromophore more rigid is a common tactic to increase the molar extinction coefficient. Rigid molecules can suppress the rotational disorder and enhance the delocalization capacity of π-electrons [30]. At the same time, however, increasing the rigidity of molecules promotes aggregation, and undesirable aggregation often adversely affects the energy conversion performance via, e.g. competitive nonradiative quenching and a hypsochromic shift of the dye [31]. As an alternative approach to enhancing the molar extinction coefficient, Ning et al. proposed incorporating an additional electron donor unit into the dye to form a starburst 2D–π–A conjugate [32]. This approach is promising for increasing light-harvesting performance; however, the number of reported starburst 2D–π–A structures is limited because of their complicated synthetic pathways. To address this problem, organoboron complexes have been investigated as relatively small and simple π-chromophore units.

The approach of incorporating organoboron complexes has been applied to a phenothiazine-based dye [30]. Phenothiazine (Figure 1.6a) is one of the most extensively studied electron-donor components and exhibits strong electron-donating character because of its heterocyclic structure containing S and N [33]. Because of its strong electron-donating ability, an early phenothiazine-based dye achieved a solar-energy-to-electricity conversion efficiency comparable to that of **N3** dye [34]. Further improving the efficiency of the phenothiazine-based dye system is difficult because of its low molar extinction coefficient. Given this background, the incorporation of organoboron complexes into phenothiazine-based dyes is attractive. In particular, 4,4-difluoro-4-bora-3*a*,4*a*-diaza-*s*-indacene (BODIPY, Figure 1.6b) dyes exhibit high molar absorptivity and sharp fluorescence peaks, along with a high QY [35]. A series of BODIPY derivatives, pyridomethene–BF_2 complexes (Figure 1.6c), exhibit a very large extinction coefficient ($5 \times 10^4 \leq \varepsilon \leq 1.4 \times 10^5\ M^{-1}\ cm^{-1}$). Among the emission quantum efficiencies of the derivatives, the highest was similar to that of **N719** [30]. To further improve BODIPY-sensitized systems, Erten-Ela et al. developed a dibenzo-BODIPY dye (Figure 1.6d) using a conventional strategy, with the objective of extending the π-conjugation and enabling longer-wavelength absorption [36]. The dibenzo-BODIPY was combined with phenothiazine (Figure 1.6e), and the absorption reached the near-infrared (NIR) region. The efficiency of BODIPY-sensitized solar cell systems eventually overtook that of **N719** systems [36]. The dibenzo-BODIPY and phenothiazine combined dye has

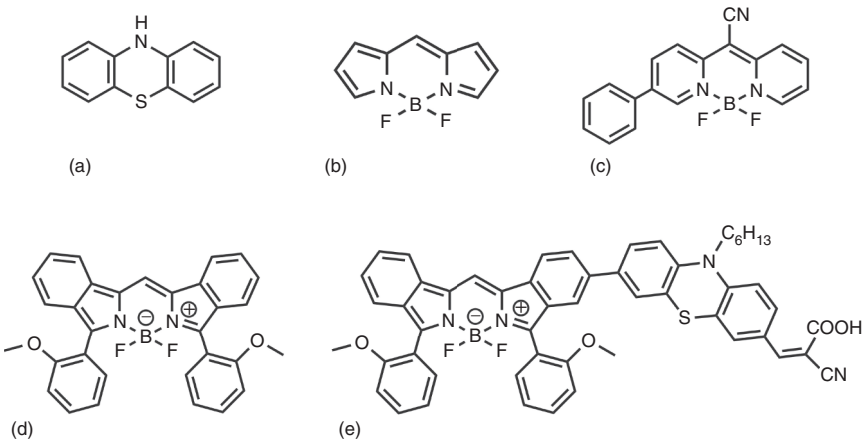

Figure 1.6 Molecular structures of (a) phenothiazine, (b) BODIPY, (c) the parent pyridomethene–BF_2 complex, (d) dibenzo-BODIPY dye, and (e) a phenothiazine dye with dibenzo-BODIPY incorporated.

been applied to the H_2-evolution reaction on Pt-modified hierarchical porous TiO_2, where ascorbic acid (AA) was used as a sacrificial electron donor [37]. The turnover number of the dye for H_2 evolution reached 11,100 under visible-light irradiation ($\lambda > 400\,\text{nm}$) at an intensity of $100\,\text{mW}\,\text{cm}^{-2}$. The organoboron-phenothiazine dye improved the visible-light absorption performance and demonstrated high H_2 evolution activity in metal-free organic dyes. That is, a binary electron donor system comprising a small and simple π-chromophore unit incorporated into an electron-donor building block functioned well as a dye-sensitized photocatalyst system.

1.2.3 Molecular Design for Efficient Excited-Charge-Carrier Separation and Injection

Efficient charge-carrier separation and injection into a semiconductor strongly affects the efficiency of a dye-sensitized system. As previously described, the visible-light absorption of dyes relies predominantly on a charge-transfer (CT) transition between donor/acceptor units. The donor unit should be physically separated from the semiconductor to suppress back electron transfer from the semiconductor and to facilitate the reaction with a reductant in the reaction solution. The acceptor unit should be physically close to the semiconductor to enable the immediate transfer of an excited electron into the semiconductor. To improve the energy conversion efficiency through the molecular design of dyes, tracing the history of the development of sensitizer molecules and understanding the roles of the building blocks of dye molecules would be beneficial. Here, a triphenylamine-based dye, which is one of the most studied organic photosensitizers, is used as an example and the history of the development of dyes is described.

Triphenylamine has been studied extensively as an electron-donor unit since the early 2000s [20]. In the earliest study of triphenylamine as a donor unit,

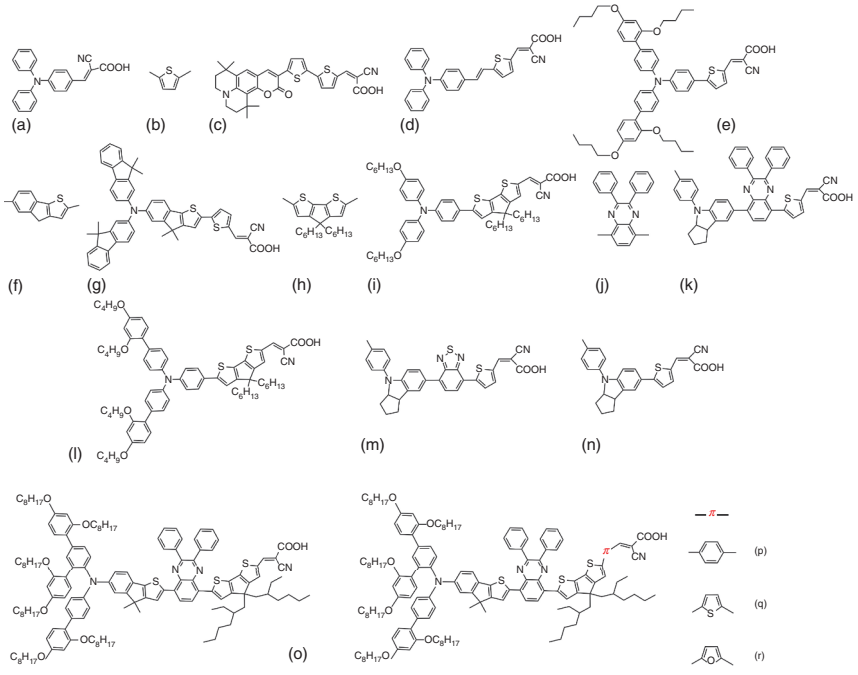

Figure 1.7 Molecular structures of (a) one of the earliest developed triphenylamine-based dyes, (b) the thiophene moiety, (c) a thiophene-bridged coumarin dye (**NKX-2677**), (d) dye **D5**, (e) dye **D35**, (f) the indeno[1,2-*b*]thiophene moiety, (g) an indeno[1,2-*b*] thiophene-bridged dye (**JK-225**), (h) the cyclopentadithiophene moiety, (i) a cyclopentadithiophene-bridged dye (**C218**), (j) a 2,3-diphenylquinoxaline unit, (k) a 2,3-diphenylquinoxaline-incorporated dye (**IQ4**), (l) **LEG4**, (m) **WS-2**, (n) **LS-1**, (o) **S5**, (p) **SD1**, (q) **SD2**, and (r) **SD3**.

dyes consisting of carboxylic and cyano moieties as electron-donor and -acceptor groups, respectively, were developed (Figure 1.7a) [18]. Because the carbon–carbon double-bonded π-bridge in these dyes is problematic in terms of the synthesis and stability of the molecule, a thiophene moiety (Figure 1.7b) was incorporated as a new π-conjugation unit to address these problems in a coumarin dye (Figure 1.7c) [38]. Combining these moieties, Hadberg et al. developed one of the simplest-structured triphenylamine-based dyes, named **D5** dye (Figure 1.7d), which gave an energy conversion efficiency comparable to that of **N719** [39]. The para-position of the triphenylamine unit was subsequently substituted to increase the electron-donating character (Figure 1.7e) [40]. Indeno[1,2-*b*]thiophene (Figure 1.7f,g) [41] and cyclopentadithiophene (Figure 1.7h,i) [42] units were used to expand the π-conjugation system. A 2,3-diphenylquinoxaline unit (Figure 1.7j,k) [43] was introduced not only as an acceptor unit but also as a building block to limit intermolecular aggregation. The use of these good building blocks (electron donor, electron acceptor, and π-conjugation units) led to the development of a triphenylamine-based D–π–A-structured dye, **LEG4** (Figure 1.7l), and its derivatives [44].

Further improvement of D–π–A-structured dyes was realized through a new molecular design: the donor–acceptor–π–acceptor (D–A–π–A) structure [45]. To explain the effects of electron–acceptor insertion between the electron-donor and π-bridge, we here discuss two dyes (**WS-2** and **LS-1**, Figure 1.7m,n, respectively) as examples. They possess an indoline-based electron donor, a thienyl π-linker, and a cyanoacrylic acid electron acceptor. The D–A–π–A dye **WS-2** has benzothiadiazole (BTD) as an additional electron acceptor. The incorporation of an electron-acceptor unit between the electron-donor and π-conjugation units influences the electronic state of the molecule, as confirmed by a density functional theory simulation of the BTD-inserted D–A–π–A dye **WS-2**. The HOMO and LUMO distributions both clearly overlap the orbitals of the BTD unit, which is beneficial for the electron transition. Comparing these two sensitizers reveals four advantages of the **WS-2** dye: (i) strong light-harvesting ability because of the bathochromic shift of the absorption associated with CT, (ii) the appearance of an additional absorption band attributed to a secondary frontier orbital transition, (iii) suppression of the hypsochromic shift that accompanies adsorption onto a TiO_2 film, and (iv) improvement of the stability for light absorption because of the decrease in the LUMO level. The substantial improvement of the light-absorption capability as a result of the formation of the D–A–π–A structure contributed to a high power conversion efficiency of 9.04% [46].

This new strategy led to the development of a derivative of the **LEG4** dye (**S5**, Figure 1.7o) [47], along with dyes with a different π-bridge, **SD1**–**3** (Figure 1.7p–r) [21]. The SD dye series was used in both DSSC and H_2-evolution DSP systems. Interestingly, the performance of the dyes was varied dramatically in the different systems. In the DSSC system, in which $[Co(bpy)_3]^{3+/2+}$ was used as an electron mediator, **SD1** exhibited the highest power conversion efficiency and the order of efficiency was **SD1** > **SD3** > **SD2**. These results are attributed to **SD1** reducing charge recombination as a result of its large torsional angle and large driving force for regenerating the dye ground state. In the DSP system, by contrast, **SD2** demonstrated the highest H_2-evolution activity on Pt/TiO_2, where AA was used as an electron donor. Spectroscopic and photoelectrochemical studies revealed that the fastest electron injection into Pt/TiO_2 and the lowest charge-carrier transfer resistance were achieved in the **SD2** system. The highest performance of **SD2** toward H_2 evolution is likely a consequence of its good electron transfer and electron–hole separation process. **SD1**, which exhibited the highest efficiency in the DSSC system, exhibited the lowest activity toward the H_2-evolution photocatalytic reaction. This different tendency is attributed to differences in the reaction conditions. The electrons injected into TiO_2 migrate to the electrode under an electrical bias in a DSSC system and are consumed by the surface H_2-evolution reaction in a DSP system. The different reaction solutions (organic solvent vs. aqueous solution) can render the dye hydrophilic or hydrophobic. The electron donor, which is the electron mediator and sacrificial reductant in each system, should influence the efficiency of the oxidation reaction. The importance of the hydrophilicity and the reaction with a reductant will be discussed in the next section.

1.2.4 Molecular Design for Facilitating the Regeneration of the Ground State

Accelerating the reduction reaction of a sensitizer in the oxidized state to regenerate the ground state is important for improving the stability of a dye because the oxidized state of a dye is decomposed via light absorption of the oxidized state itself. To investigate the influence of the electron-donor unit structure, in which the LUMO is distributed, for the regeneration reaction of the sensitizer, Bartolini et al. carried out H_2-evolution reactions using triphenylamine-based D–A–π–A dyes with and without functionalization by bulky hydrophilic substituents (Figure 1.8) [22]. **Dye1** has no special substituents on the terminal of triphenylamine, whereas **Dye2** has four bis(ethylene glycol) monomethyl ether (BEG) chains. The BEG chains improve the hydrophilicity of the sensitizer and also behave as a steric, bulky moiety. The H_2-evolution reactions were conducted in aqueous solutions containing TEOA or AA as a sacrificial electron donor (SED), and the activities were exactly opposite depending on the SED used. When TEOA was used as the SED, the H_2-evolution activity of the **Dye1** system was twofold greater than that of the **Dye2** system.

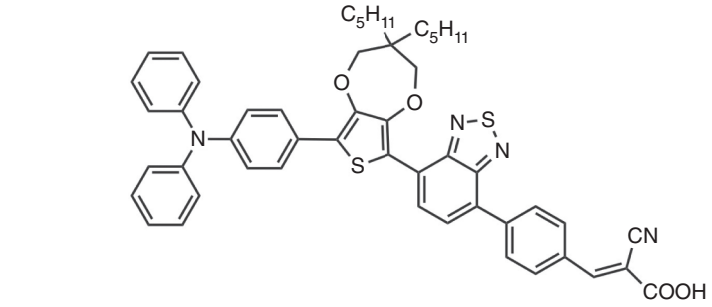

(a)

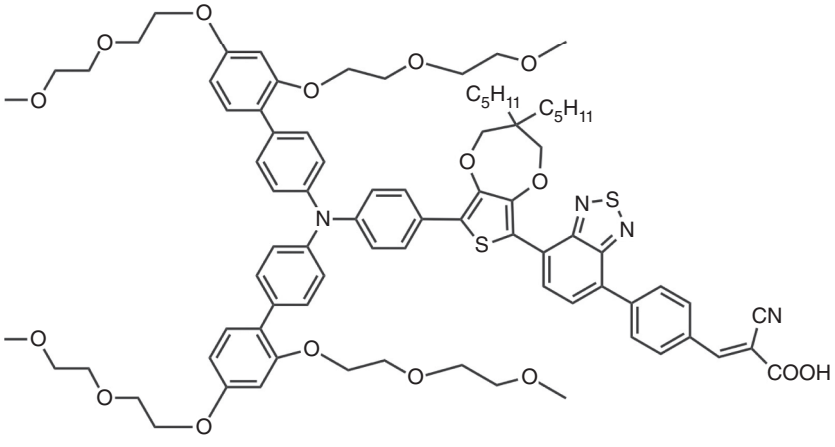

(b)

Figure 1.8 Molecular structures of (a) **Dye1** and (b) **Dye2**.

By contrast, when AA was used as the SED, the **Dye2** system exhibited twofold greater activity than the **Dye1** system. The amount of H_2 evolved when AA was used was eighteen-fold greater than that when aqueous TEOA solution was used. The large influence of the SEDs and the hydrophilic substituent on the activities can be explained in terms of the interaction between them. In the TEOA system, because no noticeable interaction occurs between the BEG chains and TEOA, such a steric bulky substituent would inhibit the access of TEOA to the electron-donor unit (triphenylamine). The suppression effect dramatically decreases the efficiency for regenerating the dye ground state, leading to very low activity for H_2 evolution. In the AA system, however, BEG chains would strongly interact with the highly polar SED, thereby accelerating the regeneration of the sensitizer ground state. That is, the hydrophilic substituent suppresses the oxidation reaction of TEOA but promotes that of AA. Therefore, a large difference in activity between the two SEDs was observed in the **Dye2** system.

The effects of hydrophobicity and hydrophilicity have also been studied in other sensitizer systems. In a carbazole-based dye system whose electron-donor unit is similar to triphenylamine, long alkoxy chains were found to improve the hydrophobicity of the dye and to increase the H_2-evolution activity in an aqueous TEOA solution [48]. Enhancing the hydrophobicity suppressed undesirable charge recombination and contributed to an improvement of the photocatalytic activity. Modification of phenothiazine with glucose through a triazole ring unit improved the hydrophilicity, thereby improving the photocatalytic H_2-evolution performance when TEOA was used as an electron donor [49]. The improvement of the activity was due to acceleration of the reaction with a reductant in aqueous solution and to suppression of intermolecular quenching, the latter of which was induced by insertion of a sterically bulky moiety. The effect of wetness around dye molecules on the excited electron-transfer process was investigated using Ru complexes [50]. Protons in water adsorbed onto the substrate oxide (TiO_2) tended to assemble around the dye molecules under dry conditions but not under wet conditions, causing instability in the oxidized form of the photosensitizer generated by electron injection. Destabilization of the oxidized dye decreased the efficiency of the electron injection.

1.2.5 Improving Stability by Forming a Strong Connection Between a Dye and a Semiconductor

A dye excited by light absorption can be desorbed from the substrate surface and/or decomposed because of its instability. The desorption and decomposition result in deactivation of the dye-sensitized system. As described in the Introduction, a dye sensitizer follows a cycle involving photoexcitation, electron injection, and regeneration. Fast regeneration of the ground state should improve the efficiency because deactivation is suppressed, as discussed in Section 1.2.4. Similarly, the excited state, which is more unstable than the oxidized form, needs to be transformed immediately to the oxidized state to improve the stability of the system; that is, fast electron injection into a semiconductor will improve the durability of a

dye-sensitized system. Robust adsorption of a dye onto a semiconductor suppresses desorption of the dye and simultaneously accelerates the electron injection via strong interaction between the sensitizer and the semiconductor. The electron-injection rate strongly depends on the electronic coupling between the density of states in the semiconductor and the electron-donating orbital of the sensitizer. In the **N3**–TiO_2 system, ultrafast electron injection was observed (~50 fs) because of the relatively high density of states of TiO_2 and favorable coupling with the electron-donating orbital (the π* orbital of the carboxyl-anchoring group of the substituted bipyridine of **N3**) [51]. Therefore, strong bonding between a dye and a semiconductor is a promising way to improve the longevity of a dye-sensitized system from the viewpoint of not only desorption but also decomposition.

A representative anchoring group used in DSSCs is the carboxyl moiety; however, the carboxyl moiety is prone to desorption in aqueous solution. A phosphonic acid moiety improves the stability in weakly acidic conditions, whereas most carboxylate-anchoring groups are desorbed at pH ≈ 6 [52]. Because metal complex dyes, especially those based on Ru(II) trisdiimine complexes, enable chemical functionalization with various ligands, the effect of the number of anchoring groups on the dyes' desorption stability and DSSC performance has been studied [52]. However, introducing multiple anchoring groups into an organic molecular dye is synthetically difficult, although the literature contains numerous reports related to multiple branching and anchoring metal-free molecular dyes [53].

A calix[4]arene-based organic dye, which is easy to synthesize and has multiple anchoring groups, was developed (Figure 1.9a) [54]. Calix[n]arene ([n]: number of units) is a ring oligomer constructed by several units that consist of methylene-substituted phenols. The four phenol units are combined with a π-conjugation unit and constitute an electron-acceptor unit. Therefore, the calix[4]arene-based dye has four D–π–A structures in one molecule. All the calix[4]arene-based dyes show a cone conformation (Figure 1.9c) with an electron-acceptor unit at the top and anchoring groups at the bottom of the cone. When this sensitizer was used as a DSSC device, the system operated for 500 hours with no degradation in performance and showed high stability under light irradiation. A calix[4]arene derivative, **HO-TPA**, was effective for DSP for the H_2-evolution and CO_2-reduction reactions (Figure 1.9b) [55]. Stable H_2-evolution activity was observed for 75 hours. The **HO-TPA** dye has calix[4]arene and triphenylamine moieties as electron-accepting and -donating units, respectively. The donor–acceptor units are conjugated by an oligothiophene moiety. This sensitizer has four –OH anchoring groups at the calix[4]arene ring, which is the conical top, and the unique structure is beneficial for suppressing dye aggregation and forming strong bonds with the substrate surface.

1.2.6 New Insights Based on the Light Harvesting of a Dye-sensitized Photocatalyst System

Dyes have been developed not only through the traditional strategy (as described in Section 1.2.1) but also through unconventional approaches based on a novel concept. To suppress dye aggregation, Manfredi et al. introduced a coadsorbent

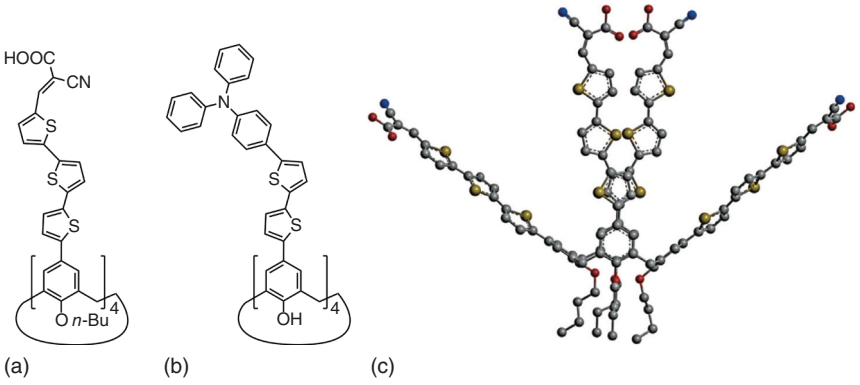

Figure 1.9 Molecular structures of (a) **Calix-3** and (b) **HO-TPA**. (c) The optimized geometry of the **Calix-3** dye was mimicked through molecular modeling with the GAUSSIAN 03 package. Source: Reproduced with permission from Tan et al. [54]; © 2015, John Wiley & Sons, Inc.

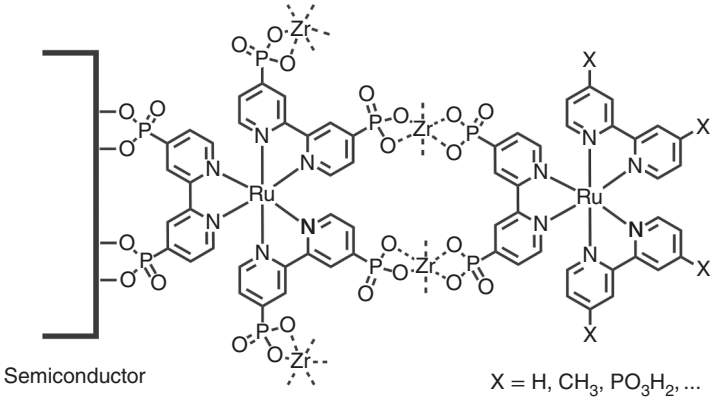

Figure 1.10 Schematic of the "layer-by-layer" assembly.

that does not function as a light absorber [56]. The H_2-evolution photocatalytic activity was doubled when the coadsorbent was adopted because it suppressed undesirable interaction among dye molecules. A direct electronic transition induced by visible light from a simple, small dye (an azoquinoline carboxylic acid) into a semiconductor (ZnO) was proposed [57]. This transition was enabled by the formation of a novel electronic state because of strong coupling between the dye and ZnO, and the transition could be used for a visible-light H_2-evolution reaction.

To effectively utilize the limited semiconductor surface, Mallouk and coworkers used a "layer-by-layer" (LBL) assembly approach [58]. This approach introduces multiple redox-active and/or chromophores onto a metal-oxide surface by forming phosphonate/Zr^{4+} coordination linkages (Figure 1.10) [59]. A bilayer assembly composed of two layers of Ru(II) complexes exhibited an approximately twofold increase in absorbance compared with a monolayer complex film. The assembly

system was successfully applied in a photocatalytic H_2-evolution system [60]. A double-layer assembly photocatalyst, which consists of two sensitizer (Ru(II) trisdiimine complex) layers and two Zr^{4+} layers, achieved ~1% of AQY for H_2 evolution under $\lambda = 470$ nm irradiation in an I_3^-/I^- redox system. The greater activity of the double-layer catalyst arose from the suppression of the back reaction ($I_3^- + 2e^- \rightarrow 2I^-$) as a result of the steric hindrance of the double layer. The adsorbed Zr^{4+} also shifted the zeta potentials of the hybrid material in the KI solution toward more negative values, suggesting that I^- anions could be attracted to the surface of the photocatalyst. This LBL assembly is a remarkable approach because it is applicable to various systems, as we will discuss later (see Section 1.4).

1.3 Semiconductor Materials

TiO_2 is one of the most studied semiconductor materials in dye-sensitized systems as well as in the heterogeneous photocatalysis community because of its synthetic versatility, relatively high optical transmittance, and high stability in aqueous solution during photoirradiation [61]. When designing semiconductors in DSP systems, three important parameters should be considered: (i) energy levels, (ii) active sites, and (iii) adsorption ability.

Semiconductors in DSP systems play roles in the transfer of electrons, which are supplied from the excited-state dye molecules, and in providing active sites for reduction reactions (e.g. H_2 evolution). Therefore, semiconductors must possess energy levels suitable for both events. The energy levels of semiconductors are, in principle, determined by their bulk properties. Maeda et al. investigated the relationships between the conduction band of semiconductors and DSP for H_2-evolution activities using calcium and strontium niobate semiconductors [62]. Their study revealed that a more negative potential of the conduction band is advantageous for H_2 evolution, although a negative conduction band adversely affects electron injection from a photosensitizer. Thus, the driving force for proton reduction was shown to be more important than that for electron injection.

Because surface catalytic reactions (H_2 or O_2 evolutions) are bottlenecks in many photocatalytic reactions, the acceleration of these reactions directly improves the photocatalytic activity. The number of active sites can be increased by introducing catalytically active nanoparticles (e.g. metals). The density of introduced nanoparticle catalysts strongly affects the DSP activity, particularly for metal-oxide semiconductors [63].

The efficient utilization of solar energy requires improving the visible-light absorption of dyes, as discussed in Section 1.2. Increasing the ability of semiconductors to adsorb dye molecules is another approach to improving the light-absorption performance of DSP systems. Numerous approaches to increasing the dye-adsorption ability of semiconductors have been reported, including modifying the surface structure (resulting in porous, hierarchical [27], and flower-like dense structures [64]), optimizing the photophysical processes [65], and introducing a

macromolecule that effectively fixes dye molecules near the active sites for H_2 evolution [66].

Recently, new materials, including carbon-based materials [67], metal–organic frameworks [68], metal phosphides [69], metal alloys [70], polyoxometalates [71] and MXenes [72], have been investigated as the semiconductor component of DSP systems. In this section, we introduce such new materials for DSP systems and discuss the effects of their active sites, dye adsorption, and energy level of the semiconductor components on the DSP systems' photocatalytic performance.

1.3.1 Crystallization of a Semicrystalline Semiconductor with Incorporation into Covalent Organic Frameworks

Similar to the development of organic dyes, numerous organic semiconductor materials have been studied for solar energy conversion systems. One class of organic materials, covalent organic frameworks (COFs), has attracted attention because of their synthetic versatility, high specific surface areas, and good physicochemical stability [73]. The crystallinity of COFs leads to long-range order, which is difficult to engineer in the case of organic materials such as conjugated polymers, whose lack of structural order often limits photoexcited charge-carrier migration. For instance, using suitable building blocks and layered stacking sequences, Wan et al. obtained a COF material with high charge-carrier mobility [74].

A planarized conjugated polymer photocatalyst that consists of a planar dibenzo [*b*,*d*]thiophene sulfone unit (Figure 1.11a) was reported, and it exhibited high H_2-evolution activity with bandgap excitation [75]. However, further improving the photocatalytic performance of this material via structural control is difficult because of its semicrystalline character. One method to utilize semicrystalline polymers is to incorporate them into COFs. Three conjugated linkers (S, FS, and TP, Figure 1.11a–c) were incorporated into the N_3-COF structure, which is active toward H_2 evolution with bandgap excitation [76], and they increased the crystallinity [73]. The physicochemical characteristics (e.g. crystal structure and water adsorption behavior) and the optical properties vary depending on the linkers in the COF structure. The FS linker (Figure 1.13b) produces FS-COF (Figure 1.13d), which was applied for the DSP for H_2 evolution by being combined with a D–A–π–A-structured indoline-based dye, **WS5F** (Figure 1.11e). The DSP system achieved 0.7% of AQY at 700 nm irradiation. The strategy of incorporating a planarized conjugated polymer building block into a COF structure is effective for engineering the physicochemical properties, and it has resulted in promising semiconductor materials for DSP systems.

1.3.2 Effect of the Number of Active Sites for Photocatalysis

Polyoxometalates (POMs) have been studied as building blocks for water-splitting photocatalyst systems because of their unique electrochemical and photochemical properties, which are advantageous for light absorption and excited-charge-carrier transfer [77]. POMs have also been investigated as a sensitizer on TiO_2 [78].

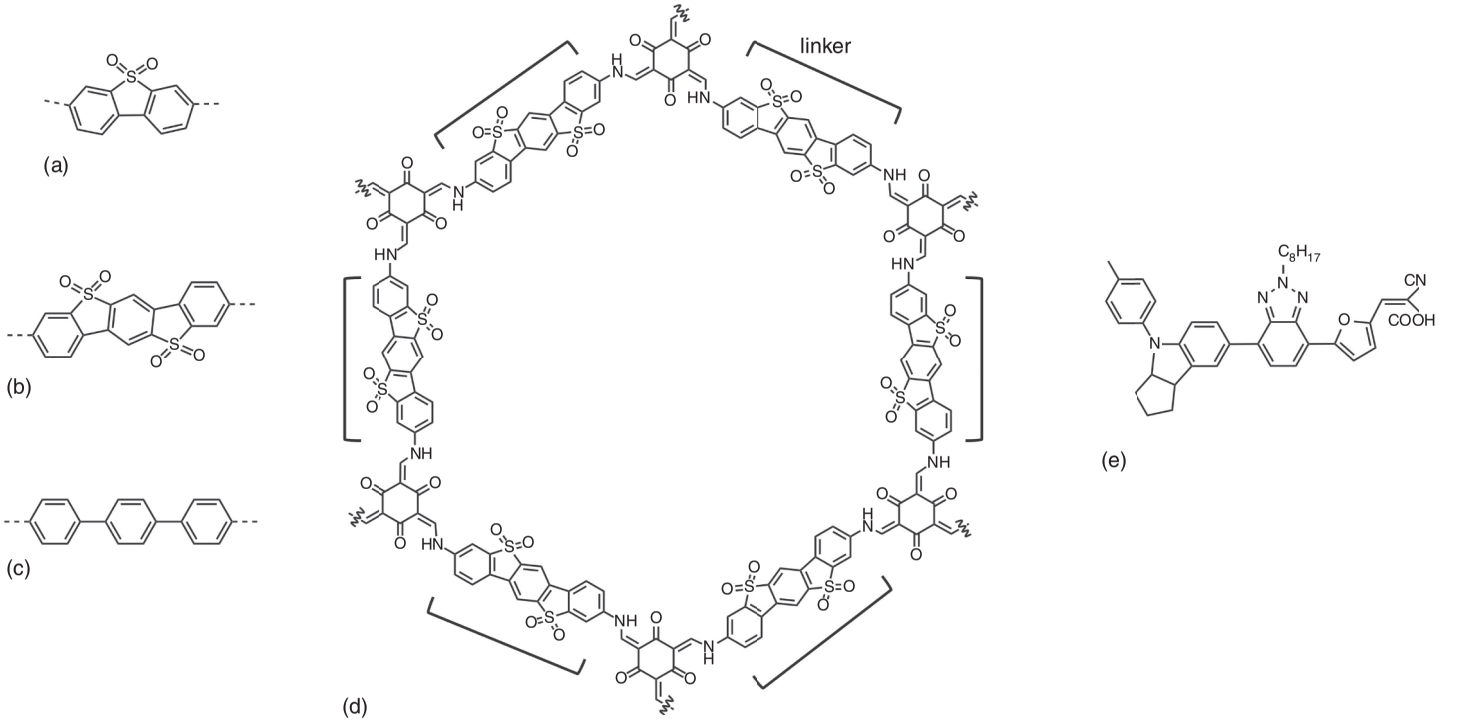

Figure 1.11 Structures of (a) S-linker, (b) FS-linker, (c) TP-linker, (d) FS-COF, and (e) **WS5F**.

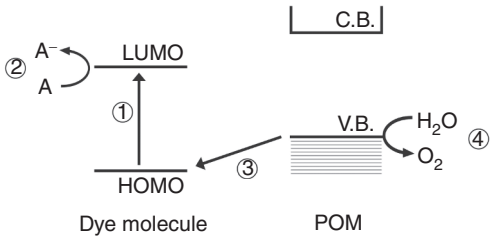

Figure 1.12 Electron transfer processes in a dye-sensitized O_2 evolution system. C.B., conduction band; V.B., valence band; HOMO, highest occupied molecular orbital; LUMO, lowest unoccupied molecular orbital; A, electron acceptor; A^-, reduced electron acceptor.

The light-absorption property of POMs can be controlled by manipulating their metal cations and their cluster sizes, and such adjustability is useful for achieving a basic understanding of their properties [79].

Exploiting the unique character of POMs enables the effect of the number of active sites to be studied, which is necessary to facilitate the surface catalytic reactions. To reveal the effect of the number of active sites, the effect of the cluster size on the DSP reaction was investigated using three molecular molybdenum-oxo materials with different sizes but with the same triclinic space group and similar light-absorption properties [80]. This system was used for DSP of the O_2-evolution reaction. The reaction flow differs from that in the H_2-evolution reaction discussed in the previous sections. As depicted in Figure 1.12, the photosensitizer first absorbs light and becomes excited (i). The excited-state dye reduces an oxidant and forms the corresponding oxidized state (ii). The light absorber in the oxidized state returns to the ground state by accepting an electron from the valence band of the semiconductor (iii). The generated hole in the semiconductor is consumed by the water oxidation reaction on the surface, and O_2 is evolved. The DSP reactions were performed by combining the POMs with tris(1,10-phenanthroline) ruthenium(II) dye, and the cationic dye and anionic POMs strongly interacted. The O_2-evolution activity was strongly dependent on the cluster size and decreased in the order α-$[Mo_8O_{26}]^{4-} > [Mo_5S_2O_{23}]^{4-} > [Mo_6O_{19}]^{2-}$. This trend corresponds well to the number of Mo_5O_t (terminal oxygen) bonds: 14 in α-$[Mo_8O_{26}]^{4-}$, 10 in $[Mo_5S_2O_{23}]^{4-}$, and 6 in $[Mo_6O_{19}]^{2-}$. These results are reasonable because the Mo_5O_t bonds in POM photocatalysts are known to be the active sites for the oxidation reaction. The use of dye-sensitized systems enables the effect of cluster size to be investigated without interference from other physicochemical properties.

1.3.3 Highly Dispersed Active-Site Molybdenum Sulfide Nanoparticles for Proton Reduction Reaction

The importance of the active sites was demonstrated in Section 1.3.2. In a heterogeneous system, the number of active sites can be increased by well dispersing catalyst (or cocatalyst) nanoparticles because highly dispersed nanoparticles have a large specific surface area. To facilitate the H_2-evolution reaction, noble metals such as Pt, Pd, and Rh have been widely used. Molybdenum sulfides are potential candidates to replace these noble-metal H_2 evolution catalysts. Amorphous MoS_x has been reported to function as a highly active water-reduction catalyst with performance comparable to that of noble metals [81].

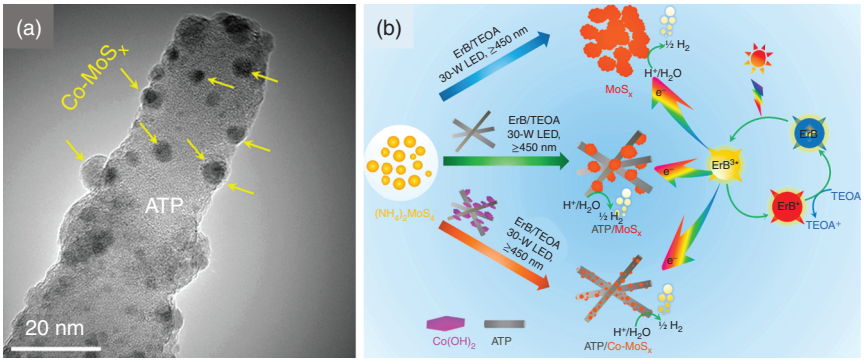

Figure 1.13 (a) HRTEM image of an ATP/Co-MoS_x catalyst. (b) Scheme of the in situ photochemical preparation of amorphous MoS_x, ATP/MoS_x, and ATP/Co-MoS_x and the photocatalytic H_2-evolution reaction. ErB: Erythrosine B photosensitizer, TEOA: triethanolamine electron donor. Source: Reproduced with permission from Liu et al. [82]; © 2018, American Chemical Society.

Amorphous and colloidal MoS_x have been applied to DSP H_2 production and have shown potential for both functioning a semiconductor and providing active sites [15, 82]. MoS_x is also known to be further activated by transition-metal doping to modulate its electronic properties, which can be carried out during in situ photodeposition [82]. The in situ growth of amorphous MoS_x, however, tends to result in its aggregation into particles as large as several hundred nanometers. To avoid aggregation, transition-metal-doped MoS_x was synthesized in situ using $Co(OH)_2$-modified attapulgite (ATP) nanofibers as starting materials. As a result, highly dispersed amorphous Co-doped MoS_x was successfully formed on ATP nanofibers (ATP/Co-MoS_x, Figure 1.13a) [82]. Notably, in situ growth without ATP or $Co(OH)_2$ resulted in micrometer-sized particles of MoS_x or ATP/MoS_x, respectively, and ATP, an insulator, served as a substrate. The photocatalytic H_2-evolution reaction was conducted in a mixed solution of Erythrosine B dye under visible light (Figure 1.13b). The activity of the ATP/Co-MoS_x was 67 and 10 times greater than that of the MoS_x particle catalyst and the ATP/MoS_x, respectively. Because the MoS_x catalysts function not only as active sites for H_2 evolution but also as an electron-conductive substrate in this system, highly dispersed MoS_x promotes electron transfer from the excited Erythrosine B dyes.

1.3.4 Improving the Solar Energy Conversion Efficiency by Suppressing Undesirable Backward Reactions

Introducing active sites for a catalytic reaction can accelerate not only the forward reactions but also undesirable backward reactions. In the case of the DSP half-reaction, the backward reaction is re-reduction or re-oxidation of a reversible electron donor, e.g. re-reduction of I_3^- in I_3^-/I^- redox system. Because such backward redox reactions are usually thermodynamically favored over the catalytic formation of H_2 or O_2, these reactions often dominate the efficiency of the

whole system. When a photocatalysis system evolves H_2 and O_2 simultaneously, the backward reaction of water formation from them should also be suppressed because a proton-reduction catalyst usually promotes the backward reaction. Overall water splitting is often achieved in a two-step excitation system: the so-called Z-scheme. In the Z-scheme process, two semiconductors catalyze H_2 and O_2 evolution, whereas a redox shuttle reagent mediates electron transfer between the two photocatalysts. Therefore, suppressing the undesirable reactions is paramount for improving the solar energy conversion efficiency.

A straightforward method to suppress backward reactions involving more reducible or oxidizable products is physical separation of the products from the active sites for forward reactions [83]. In the case of Pt-loaded layered oxide semiconductors, Pt nanoparticles are intercalated into the layers of the oxide. Protons can reach the intercalated Pt, whereas I_3^- ions cannot because of their large size. Researchers have also confirmed that the intercalation of Pt catalysts inhibits H_2–O_2 recombination [84]. The backward reaction of I_3^- to I^- was also found to be inhibited by surface modification using poly(styrenesulfonate), which led to as much as a fivefold improvement of the H_2-evolution activity compared with that of the unmodified catalyst [85]. An amide-functionalized reduced graphene oxide (RGO) modified with Pt could function as a good building block for DSP H_2 evolution [86]. Because the functionalized amide groups strongly adsorb O_2 molecules as a result of orbital hybridization between an N 2*p* orbital of the amide group and an O 2p orbital of an O_2 molecule, the concentration of dissolved O_2 molecules in the reaction solution was decreased and the backward water formation reaction was suppressed on Pt.

Backward electron transfer events other than the redox reactions should also be considered as undesirable processes in the DSP cycle. Back electron transfer occurs at the origin of injected electrons in the conduction band. The electrons in the semiconductor can drive the reduction reaction of the photosensitizers in the oxidized state. Nishioka et al. achieved inhibition of back electron transfer by modifying the semiconductor surface with Al_2O_3 [87]. The effect of Al_2O_3 was investigated by transient absorption measurement, which revealed that the suppression arises from physical separation of the adsorbed dye from the semiconductor. Notably, injection of the excited electron into the semiconductor was hardly affected by the Al_2O_3 modification, whereas the back electron transfer process was clearly inhibited.

Oshima et al. combined these two physical separation processes for suppressing the backward reaction with an electron mediator and the back electron transfer to develop a dye-sensitized photocatalyst [84]. The catalyst comprised calcium niobate nanosheets intercalated with a Pt cocatalyst for H_2 evolution and further modified with an Al_2O_3 layer. The Z-scheme water-splitting reaction was performed using a Ru(II) trisdiimine complex sensitizer combined with a PtO_x/H–Cs–WO_3 water-oxidation photocatalyst (Figure 1.14). The photocatalyst system achieved an AQY of 2.4% for water splitting under visible-light irradiation, which is the highest AQY reported to date for a dye-sensitized overall water-splitting system.

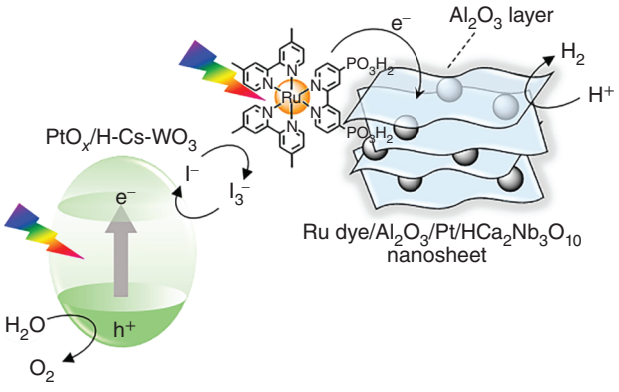

Figure 1.14 Schematic of Z-scheme water splitting using Ru dye-sensitized Al_2O_3/Pt/$HCa_2Nb_3O_{10}$ nanosheets and PtO_x/H–Cs–WO_3. Source: Reproduced with permission from Oshima et al. [84]; © 2020, American Chemical Society.

1.3.5 Immobilization of Dyes on a Reduced Graphene Oxide Surface Through Formation of Chemical Bonds

Graphene-based materials are among the most attractive conducting materials. Graphene has been used in electron-conductive devices because of its unusual properties, which include a high specific surface area, high intrinsic mobility, and high optical transmittance [88]. The oxidized form, graphene oxide (GO), is highly hydrophilic and can be suspended in an aqueous environment. The trade-off for hydrophilicity, however, is that GO lacks sufficiently high conductivity because of the disruption of the "graphitic" networks of graphene [89]. The electrical conductivity can be restored by reducing GO to form RGO. RGO possesses a substantial amount of O atoms in its structure (atomic C/O ratio: ~10), and its properties clearly differ from those of pristine graphene [89]. Because of its properties, RGO can be well dispersed in aqueous solutions and exhibits moderate electrical conductivity. Because these properties are beneficial for the water-splitting reaction, RGO has been applied as a conductor building block for H_2-evolution DSP systems [90, 91].

The organic texture of RGO enables dye molecules to be immobilized on their surface through the formation of chemical bonds. A silicon phthalocyanine dye (**SiPc**) was stabilized on N-doped RGO (N-RGO) by forming O–Si–O bonds with the O atom of a phenol moiety as a result of treating N-RGO with *N*-methyl glycine and 4-formylphenol [90]. The formation of a chemical bond between a dye and a semiconductor improves the electron-injection efficiency and the stability between them. An **SiPc**- and Pt-comodified N-RGO hybrid photocatalyst showed stable H_2-evolution activity for more than 30 hours. Similar chemical bond formation between the RGO and dye was performed in an RGO-**N749** system [91]. **N749** dyes were combined with RGO through an amine-terminated six-armed polyethylene glycol moiety. Because of the chemical bonding, the hybrid material showed high stability for 30 hours of photocatalytic reaction, similar to the stability of the **SiPc**–RGO system. The H_2 evolution activity of the hybrid material, however, was

poor: less than 1% of the AQY for the H_2-evolution half-reaction under visible-light irradiation. The moderate photocatalytic activities likely arose from the difficulty of engineering energy levels as a result of the loss of the semiconductive character.

1.3.6 Metal Phospho-Sulfides and -Selenides as Electron-Conducting and Proton-Adsorbing Materials

Metal phosphide nanomaterials have recently attracted attention as electrocatalysts and photocatalysts. A bimetallic phosphide can generate H_2 and O_2 in different DSP systems (i.e. Eosin-Y sensitization for H_2 and $[Ru(bpy)_3]^{2+}$ sensitization for O_2 evolution) [92]. An important role of phosphorus is the attraction of the proton to the surface of a metal phosphide. Increasing the ratio of phosphorus in a metal phosphide increases its electrochemical H_2-evolution activity [93]. For use in semiconductor photocatalysis, metal phospho-sulfides and -selenides (MPX_3, M = metal, X = S, Se) showing semiconducting behavior with 1.2–3.4 eV bandgaps have been developed [94]. As the metal in MPX_3, divalent cations (V^{2+}, Mn^{2+}, Fe^{2+}, Co^{2+}, Ni^{2+}, Zn^{2+}, Cd^{2+}, Sn^{2+}, or Hg^{2+}) for the M^{2+} system ($M^{2+}PX_3$) or monovalent cations (Ag^+ or Cu^+) and trivalent cations (Cr^{3+}, V^{3+}, Al^{3+}, Ga^{3+}, In^{3+}, or Bi^{3+}) for the $M^{1+} + M^{3+}$ system ($M^{1+}_{0.5}M^{3+}_{0.5}PX_3$) have been reported [95]. Ten types of MPX_3 (M = Ag^+, Ni^{2+}, Fe^{2+}, Cd^{2+}, Mn^{2+}, Zn^{2+}, In^{3+}; X = S, Se) were synthesized and used in DSP systems with Eosin-Y as a dye sensitizer. The activities were strongly dependent on the metal cation. The investigation led to three main findings: the activity was enhanced with (1) decreasing energy of the conduction-band minimum, (2) decreasing free energy for the adsorption of protons, and (3) decreasing P—P bond length. Trend (1) is opposite that of the Ru(II) complex–niobate-based nanosheet hybrid system mentioned in the introduction of this section [62], likely reflecting the difference in the reactions. In the case of Ru(II) complexes, they are chemically adsorbed onto the nanosheets and the electron injection occurs quickly from the adsorbed sensitizer upon photoexcitation. However, in the case of MPX_3, the H_2-evolution reaction was conducted in a physical mixture of MPX_3 and Eosin-Y. In this case, dye-to-MPX_3 electron injection appears to be slow compared with that in the hybridized system. Point (2), enhanced activity with decreasing free energy for the adsorption of protons, is well consistent with the metal phosphide catalyst, as previously described. Point (3), related to the P—P bond length, influences the electron density at each P center, which is the active site for the H_2-evolution reaction [94]. The antibonding levels of the P—P bond constitute the conduction band with the *s* and *p* orbitals of the metal. An increase in the P—P bond length leads to a decrease in the electron density at the P center, weakening the orbital overlap with the *s* and *p* orbitals of the metal (i.e. increasing the potential of the conduction band minimum). As a result, the activity is reduced.

1.3.7 Effects of Dye Adsorption for the Electronic State of the Semiconductor

As described in Section 1.2, strong electronic interaction between a semiconductor and the adsorbed sensitizer will affect the absorption of the dye and is the origin of

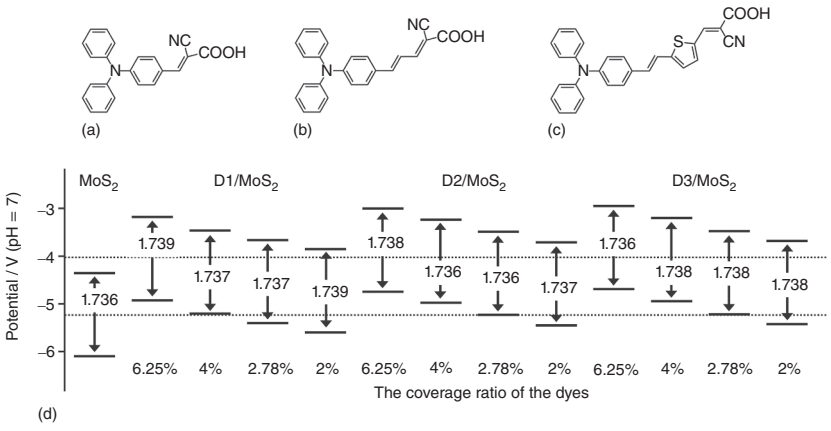

Figure 1.15 Molecular structures of (a) **D1**, (b) **D2**, and (c) **D3**. (d) Calculated band potentials of MoS_2 and dye-adsorbed MoS_2 with different dye coverage ratios. Source: Reproduced with permission from Pan et al. [96]; © 2020, American Chemical Society.

the very fast excited-electron injection that occurs on a timescale of femtoseconds to picoseconds. Such strong coupling should also influence the electronic state of the semiconductor. Because the bulk properties of the semiconductor would not be influenced even by the very strong interaction, a two-dimensional material is suitable to investigate the effect of an adsorbed dye on the semiconductor properties. By employing a monolayer of molybdenum sulfide as the semiconductor and three triphenylamine-based dyes, Pan et al. studied the electronic interaction between the two components through computational modeling and calculations (Figure 1.15a–c) [96]. The band edges of MoS_2 were shifted negatively by dye adsorption, and the degree of the negative shift increased with increasing intrinsic dipoles of the sensitizer (Figure 1.15d). These negative shifts could also be controlled by the surface coverage of the molecular dye. The band-edge potentials of monolayer MoS_2, which were originally not suitable for the water-splitting reaction, were found to straddle the water reduction/oxidation potentials upon dye adsorption. The calculation results suggested that dye adsorption varies the band potential of MoS_2, at least on the surface, even for bulky MoS_2.

1.4 Dye-sensitized Photocatalysts in Electrochemical Systems

Dye-sensitized photocatalysts have been applied in a photoelectrochemical cell that produces H_2 and O_2 from water [97–101]. There are two types of photoelectrochemical water-splitting cells: a water-oxidation photoanode [97–99] and a water-reduction photocathode [100, 101]. For a photoanode, dye-sensitized *n*-type semiconductors (e.g. TiO_2) are used as an electron-conductive substrate (Figure 1.16a). The injected electrons in TiO_2 migrate to the counter electrode through an external circuit because of upward band bending formed at the semiconductor–solution interface and are finally consumed to reduce water to H_2.

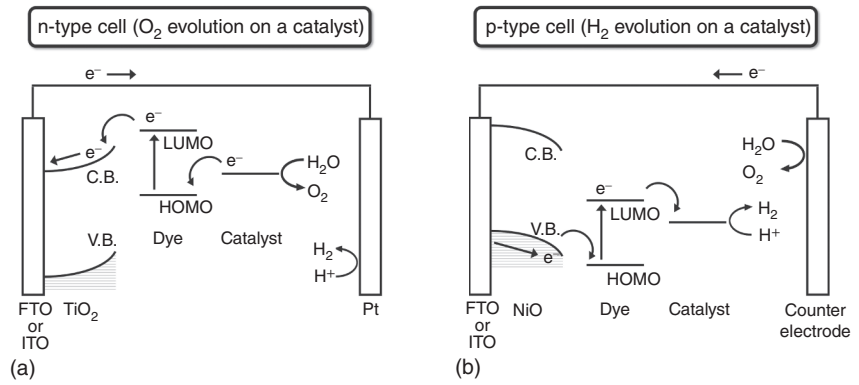

Figure 1.16 Schematic of water-splitting dye-sensitized (a) n-type and (b) p-type cells.

The oxidized sensitizer must accept an electron from water for O_2 evolution, hence necessitating a catalyst. For a photocathode, by contrast, dye-sensitized *p*-type semiconductors (e.g. NiO) are used (Figure 1.16b). The excited electrons in the dye are transferred to the catalyst and expended to reduce a proton for H_2 evolution. The oxidized dye receives an electron from the *p*-type semiconductor and returns to the ground state. The electrons are generated through the water oxidation reaction on the counter electrode and are transported via the external circuit. These are typical dye-sensitized photoelectrochemical water-splitting cycles.

To promote the catalytic reactions on the photoelectrodes, two main strategies have been studied. One strategy is to incorporate a catalyst into the photosensitizer [97, 100]. Another is to hybridize the dye and a molecular catalyst [99, 101]. In the case of catalyst–dye integration, cocatalysts for water splitting (e.g. IrO_x for O_2 evolution, Pt and Pd for H_2 evolution) are often selected as the catalyst. A colloidal IrO_2 water oxidation catalyst was adsorbed onto a photosensitizer with a dimethylmalonyl-anchoring moiety, which is not used for adsorbing dye molecules onto TiO_2 electrodes [97]. Although this photoanode functioned as a water-oxidation photoelectrode, the reaction efficiency was not sufficient because the forward electron transfer from IrO_2 into the photosensitizer was much slower than the undesirable electron transfers (i.e. electron transfers from TiO_2 into the oxidized dye and from the excited dye into IrO_2).

Pt and Pd catalysts incorporated into photosensitizers have been developed as water-reduction photocathodes [100]. Pt and Pd metal centers were integrated by forming a chemical bond with a ligand of the sensitizer. Although the integration of a metal center and dye improved the photoelectrochemical H_2-evolution activity compared with that of a system with separated dyes and catalysts, it required a large applied electrochemical bias for efficient catalytic reaction. This requirement is due to the undesirable electron transfer processes, similar to the case of the IrO_2 water-oxidation photoanode.

To avoid the unwanted electron transfer, physical separation between an electron- and a hole- collector is one of the effective approaches. The LBL assembly technique has been widely used, as described in Section 1.2.6 [99]. The LBL photoanodes

contained a conductive indium tin oxide electrode (semiconductor), methyl viologen (electron acceptor), Ru(II) trisdiimine complex (light absorber), Fe(II) bisterpyridine complex (electron donor), and Ru(II) water oxidation catalyst (Figure 1.17). The physical separation clearly inhibited the undesirable electron transfer events. Furthermore, the insertion of the electron acceptor between the electrode and the light absorber promoted the forward electron injection. The maximum value of incident photon-to-current efficiency reached 2.3% at 440 nm for the water-oxidation reaction, indicating that the physical separation strategy worked on a water-oxidation photoanode system. In addition, a noticeable feature of the method is its usability for both the photoanode and the photocathode depending on the structural design, even if the same light absorber is employed [102].

Notably, dye-sensitized photocathodes have been used in CO_2 reduction systems based on LBL assembly [103] and a highly stable metal-complex polymer [104]. The Ru-complex polymer system achieved CO_2 reduction in water and simultaneous O_2 evolution without any applied electrical bias [104]. This remarkable accomplishment demonstrates the promise of photoelectrosynthesis for advancing solar energy conversion.

1.5 Conclusion

We here reviewed recent progress in dye-sensitized photocatalysis, with focus on the building blocks, which are light absorbers and semiconductor materials. Important factors and strategies to improve the photocatalytic performance were discussed for each building block. For the molecular design of light absorbers, there are two significant trade-off relationships: Narrowing the HOMO–LUMO gap for longer-wavelength absorption adversely affects the electron transfer and redox processes because the driving force for these reactions is diminished, whereas strengthening the dye adsorption to improve stability can adversely affect the energy conversion efficiency because the backward electron transfer may be also accelerated. These difficult problems can be remedied by the following strategies. To intensify the light absorption, the incorporation of a chemical unit with a large molar extinction coefficient into the light absorber or forming multiple layers of light absorbers is effective. To attain robust adsorption, the important point is not reinforcement of the bonding but coordination with multidentate ligands. For the semiconductor component, we focused on new materials as potential alternatives to the standard material, TiO_2. Numerous new electron-conductive materials applicable to dye-sensitized H_2 evolution have been reported. COFs and metal–phospho-sulfides are promising materials for the DSP system. Methods of promoting the forward reactions and suppressing the backward reactions were discussed with a focus on the active sites. In the last section, dye-sensitized photoelectrochemical cells were introduced as a promising technology for solar energy conversion applications.

As previously described, because numerous factors strongly influence the energy conversion efficiency of DSP systems, improving the systems is not simple. Conversely, numerous factors influence the efficiency, suggesting that dramatic

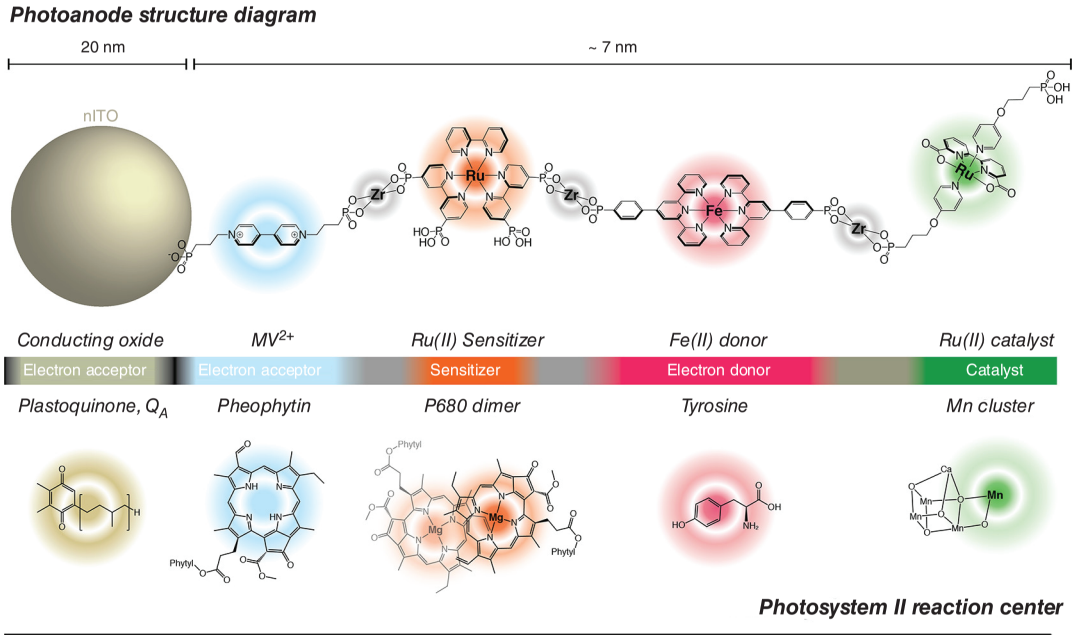

Figure 1.17 Structure of the molecular assembly of the four-molecular layer-by-layer photoanode and a diagram showing the key functional components of Photosystem II. Source: Reproduced with permission from Wang et al. [99]; © 2019, American Chemical Society.

improvements in DSP systems can be reasonably expected when many factors are understood and controlled. Such improvements require in-depth, detailed studies; for example, a kinetic study can reveal bottlenecks in a DSP system. Whereas kinetic studies have been extensively conducted in the DSSC field, the literature contains few detailed reports related to DSP systems. This dearth of information is attributable to the difficulty associated with using spectroscopic measurements to characterize DSP systems, a consequence of the reaction conditions, which typically involve a suspension. Powder suspension systems are basically not suitable for spectroscopic measurement. With improvements in the measurement techniques and analysis methods, however, some kinetic studies have been reported [105–107]. In the future, additional efforts should be devoted to understanding the reaction mechanisms in the dye-sensitized photocatalysis field.

References

1 Gerischer, H. (1972). Electrochemical techniques for the study of photosensitization. *Photochem. Photobiol.* 16: 243–260.

2 Borgarello, E., Kiwi, J., Pelizzettit, E. et al. (1981). Photochemical cleavage of water by photocatalysis. *Nature* 289: 158–160.

3 Reginato, G., Zani, L., Calamante, M. et al. (2020). Dye-sensitized heterogeneous photocatalysts for green redox reactions. *Eur. J. Inorg. Chem.* 2020: 899–917.

4 Brennaman, M.K., Dillon, R.J., Alibabaei, L. et al. (2016). Finding the way to solar fuels with dye-sensitized photoelectrosynthesis cells. *J. Am. Chem. Soc.* 138: 13085–13102.

5 Willkomm, J., Orchard, K.L., Reynal, A. et al. (2016). Dye-sensitised semiconductors modified with molecular catalysts for light-driven H_2 production. *Chem. Soc. Rev.* 45: 9–23.

6 Matsumura, M., Nomura, Y., and Tsubomura, H. (1977). Dye-sensitization on the photocurrent at zinc oxide electrode in aqueous electrolyte solution. *Bull. Chem. Soc. Jpn.* 50: 2533–2537.

7 O'Regan, B. and Grätzel, M. (1991). A low-cost, high-efficiency solar cell based on dye-sensitized colloidal TiO_2 films. *Nature* 353: 737–740.

8 Amadelli, R., Argazzi, R., Bignozzi, C.A., and Scandola, F. (1990). Design of antenna-sensitizer polynuclear complexes. Sensitization of titanium dioxide with $[Ru(bpy)_2(CN)_2]_2Ru(bpy(COO)_2)_2^{2-}$. *J. Am. Chem. Soc.* 112: 7099–7103.

9 Nazeeruddin, M.K., Kay, A., Rodicio, I. et al. (1993). Conversion of light to electricity by *cis*-X_2bis(2,2′-bipyridyl-4,4′-dicarboxylate)ruthenium(II) charge-transfer sensitizers (X=Cl^-, Br^-, I^-, CN^-, and SCN^-) on nanocrystalline TiO_2 electrodes. *J. Am. Chem. Soc.* 115: 6382–6390.

10 Nazeeruddin, M.K., Zakeeruddin, S.M., Humphry-Baker, R. et al. (1999). Acid-base equilibria of (2,2′-bipyridyl-4,4′-dicarboxylic acid)ruthenium(II) complexes and the effect of protonation on charge-transfer sensitization of nanocrystalline titania. *Inorg. Chem.* 38: 6298–6305.

11 Nazeeruddin, M.K., Splivallo, R., Liska, P. et al. (2003). A swift dye uptake procedure for dye sensitized solar cells. *Chem. Commun.* 12: 1456–1457.

12 Zhang, X., Veikko, U., Mao, J. et al. (2012). Visible-light-induced photocatalytic hydrogen production over binuclear Ru^{II}-bipyridyl dye-sensitized TiO_2 without noble metal loading. *Chem. Eur. J.* 18: 12103–12111.

13 Swetha, T., Mondal, I., Bhanuprakash, K. et al. (2015). First study on phosphonite-coordinated ruthenium sensitizers for efficient photocatalytic hydrogen evolution. *ACS Appl. Mater. Interfaces* 7: 19635–19642.

14 Wang, J., Zheng, Y., Peng, T. et al. (2017). Asymmetric zinc porphyrin derivative-sensitized graphitic carbon nitride for efficient visible-light-driven H_2 production. *ACS Sustain. Chem. Eng.* 5: 7549–7556.

15 Yuan, Y.J., Yu, Z.T., Liu, X.J. et al. (2014). Hydrogen photogeneration promoted by efficient electron transfer from iridium sensitizers to colloidal MoS_2 catalysts. *Sci. Rep.* 4: 4045.

16 Hirata, N., Lagref, J.J., Palomares, E.J. et al. (2004). Supramolecular control of charge-transfer dynamics on dye-sensitized nanocrystalline TiO_2 films. *Chem. Eur. J.* 10: 595–602.

17 Jayaweera, P.M., Kumarasinghe, A.R., and Tennakone, K. (1999). Nano-porous TiO_2 photovoltaic cells sensitized with metallochromic triphenylmethane dyes: [n-TiO_2/triphenylmethane dye/p-I^-/I_3^- (or CuI)]. *J. Photochem. Photobiol. A Chem.* 126: 111–115.

18 Kitamura, T., Ikeda, M., Shigaki, K. et al. (2004). Phenyl-conjugated oligoene sensitizers for TiO_2 solar cells. *Chem. Mater.* 16: 1806–1812.

19 Hagfeldt, A., Boschloo, G., Sun, L. et al. (2010). Dye-sensitized solar cells. *Chem. Rev.* 110: 6595–6663.

20 Mahmood, A. (2016). Triphenylamine based dyes for dye sensitized solar cells: a review. *Sol. Energy* 123: 127–144.

21 Ding, H., Chu, Y., Xu, M. et al. (2020). Effect of π-bridge groups based on indeno[1,2-*b*] thiophene D-A-π-A sensitizers on the performance of dye-sensitized solar cells and photocatalytic hydrogen evolution. *J. Mater. Chem. C* 8: 14864–14872.

22 Bartolini, M., Gombac, V., Sinicropi, A. et al. (2020). Tuning the properties of benzothiadiazole dyes for efficient visible light-driven photocatalytic H_2 production under different conditions. *ACS Appl. Energy Mater.* 3: 8912–8928.

23 Celil Yüzer, A., Genc, E., Harputlu, E. et al. (2020). Subphthalocyanine-sensitized TiO_2 photocatalyst for photoelectrochemical and photocatalytic hydrogen evolution. *Dalt. Trans.* 49: 12550–12554.

24 Abe, R., Shinmei, K., Koumura, N. et al. (2013). Visible-light-induced water splitting based on two-step photoexcitation between dye-sensitized layered niobate and tungsten oxide photocatalysts in the presence of a triiodide/iodide shuttle redox mediator. *J. Am. Chem. Soc.* 135: 16872–16884.

25 Yu, F., Wang, Z., Zhang, S. et al. (2018). N-annulated perylene-based organic dyes sensitized graphitic carbon nitride to form an amide bond for efficient photocatalytic hydrogen production under visible-light irradiation. *Appl. Catal. B Environ.* 237: 32–42.

26 Huang, J.F., Liu, J.M., Xiao, L.M. et al. (2019). Facile synthesis of porous hybrid materials based on Calix-3 dye and TiO_2 for high photocatalytic water splitting performance with excellent stability. *J. Mater. Chem. A* 7: 2993–2999.

27 Tiwari, A., Duvva, N., Rao, V.N. et al. (2019). Tetrathiafulvalene scaffold-based sensitizer on hierarchical porous TiO_2: efficient light-harvesting material for hydrogen production. *J. Phys. Chem. C* 123: 70–81.

28 Nazeeruddin, M.K., Péchy, P., Renouard, T. et al. (2001). Engineering of efficient panchromatic sensitizers for nanocrystalline TiO_2-based solar cells. *J. Am. Chem. Soc.* 123: 1613–1624.

29 Kinoshita, T., Dy, J.T., Uchida, S. et al. (2013). Wideband dye-sensitized solar cells employing a phosphine-coordinated ruthenium sensitizer. *Nat. Photonics* 7: 535–539.

30 Lin, Y.-D., Ke, B.-Y., Chang, Y.J. et al. (2015). Pyridomethene-BF_2 complex/phenothiazine hybrid sensitizer with high molar extinction coefficient for efficient, sensitized solar cells. *J. Mater. Chem. A* 3: 16831–16842.

31 Zhang, L. and Cole, J.M. (2017). Dye aggregation in dye-sensitized solar cells. *J. Mater. Chem. A* 5: 19541–19559.

32 Ning, Z., Zhang, Q., Wu, W. et al. (2008). Starburst triarylamine based dyes for efficient dye-sensitized solar cells. *J. Org. Chem.* 73: 3791–3797.

33 Huang, Z.-S., Meier, H., and Cao, D. (2016). Phenothiazine-based dyes for efficient dye-sensitized solar cells. *J. Mater. Chem. C* 4: 2404–2426.

34 Tian, H., Yang, X., Chen, R. et al. (2007). Phenothiazine derivatives for efficient organic dye-sensitized solar cells. *Chem. Commun.* 3741–3743.

35 Loudet, A. and Burgess, K. (2007). BODIPY dyes and their derivatives: Syntheses and spectroscopic properties. *Chem. Rev.* 107: 4891–4932.

36 Erten-Ela, S., Ueno, Y., Asaba, T., and Kubo, Y. (2017). Synthesis of a dibenzo-BODIPY-incorporating phenothiazine dye as a panchromatic sensitizer for dye-sensitized solar cells. *New J. Chem.* 41: 10367–10375.

37 Suryani, O., Higashino, Y., Sato, H., and Kubo, Y. (2019). Visible-to-near-infrared light-driven photocatalytic hydrogen production using dibenzo-bodipy and phenothiazine conjugate as organic photosensitizer. *ACS Appl. Energy Mater.* 2: 448–458.

38 Hara, K., Kurashige, M., Dan-Oh, Y. et al. (2003). Design of new coumarin dyes having thiophene moieties for highly efficient organic-dye-sensitized solar cells. *New J. Chem.* 27: 783–785.

39 Hagberg, D.P., Edvinsson, T., Marinado, T. et al. (2006). A novel organic chromophore for dye-sensitized nanostructured solar cells. *Chem. Commun.* 2245–2247.

40 Hagberg, D.P., Jiang, X., Gabrielsson, E. et al. (2009). Symmetric and unsymmetric donor functionalization. comparing structural and spectral benefits of chromophores for dye-sensitized solar cells. *J. Mater. Chem.* 19: 7232–7238.

41 Lim, K., Kim, C., Song, J. et al. (2011). Enhancing the performance of organic dye-sensitized solar cells via a slight structure modification. *J. Phys. Chem. C* 115: 22640–22646.

42 Li, R., Liu, J., Cai, N. et al. (2010). Synchronously reduced surface states, charge recombination, and light absorption length for high-performance organic dye-sensitized solar cells. *J. Phys. Chem. B* 114: 4461–4464.

43 Pei, K., Wu, Y., Islam, A. et al. (2013). Constructing high-efficiency D-A-π-A-featured solar cell sensitizers: A promising building block of 2,3-diphenylquinoxaline for antiaggregation and photostability. *ACS Appl. Mater. Interfaces* 5: 4986–4995.

44 Gabrielsson, E., Ellis, H., Feldt, S. et al. (2013). Convergent/divergent synthesis of a linker-varied series of dyes for dye-sensitized solar cells based on the D35 donor. *Adv. Energy Mater.* 3: 1647–1656.

45 Wu, Y. and Zhu, W. (2013). Organic sensitizers from D–π–A to D–A–π–A: Effect of the internal electron-withdrawing units on molecular absorption, energy levels and photovoltaic performances. *Chem. Soc. Rev.* 42: 2039–2058.

46 Wu, Y., Marszalek, M., Zakeeruddin, S.M. et al. (2012). High-conversion-efficiency organic dye-sensitized solar cells: Molecular engineering on D-A-π-A featured organic indoline dyes. *Energy Environ. Sci.* 5: 8261–8272.

47 Shen, Z., Xu, B., Liu, P. et al. (2017). High performance solid-state dye-sensitized solar cells based on organic blue-colored dyes. *J. Mater. Chem. A* 5: 1242–1247.

48 Watanabe, M., Hagiwara, H., Ogata, Y. et al. (2015). Impact of alkoxy chain length on carbazole-based, visible light-driven, dye sensitized photocatalytic hydrogen production. *J. Mater. Chem. A* 3: 21713–21721.

49 Manfredi, N., Cecconi, B., Calabrese, V. et al. (2016). Dye-sensitized photocatalytic hydrogen production: distinct activity in a glucose derivative of a phenothiazine dye. *Chem. Commun.* 52: 6977–6980.

50 Ishizaki, R., Fukino, R., Matsuzaki, H., and Katoh, R. (2017). Effect of adsorbed water molecules on light harvesting and electron injection processes in dye-sensitized nanocrystalline TiO_2 films. *J. Phys. Chem. C* 121: 16266–16274.

51 Asbury, J.B., Hao, E., Wang, Y. et al. (2001). Ultrafast electron transfer dynamics from molecular adsorbates to semiconductor nanocrystalline thin films. *J. Phys. Chem. B* 105: 4545–4557.

52 Park, H., Bae, E., Lee, J.J. et al. (2006). Effect of the anchoring group in Ru-bipyridyl sensitizers on the photoelectrochemical behavior of dye-sensitized TiO_2 electrodes: carboxylate versus phosphonate linkages. *J. Phys. Chem. B* 110: 8740–8749.

53 Manfredi, N., Cecconi, B., and Abbotto, A. (2014). Multi-branched multi-anchoring metal-free dyes for dye-sensitized solar cells. *European J. Org. Chem.* 7069–7086.

54 Tan, L., Liu, J., Li, S. et al. (2015). Dye-sensitized solar cells with improved performance using cone-Calix[4]arene based dyes. *ChemSusChem* 8: 280–287.

55 Chen, Y., Huang, J., Shen, M. et al. (2019). A porous hybrid material based on calixarene dye and TiO_2 demonstrating high and stable photocatalytic performance. *J. Mater. Chem. A* 7: 19852–19861.

56 Manfredi, N., Monai, M., Montini, T. et al. (2018). Dye-sensitized photocatalytic hydrogen generation: Efficiency enhancement by organic photosensitizer-coadsorbent intermolecular interaction. *ACS Energy Lett.* 3: 85–91.

57 George, L., Sappati, S., Ghosh, P., and Devi, R.N. (2018). Sensitizing with short conjugated molecules: Multimodal anchoring on ZnO nanoparticles for enhanced electron transfer characteristics, stability and H_2 evolution. *Catal. Today* 309: 89–97.

58 Lee, H., Kepley, L.J., Hong, H.G., and Mallouk, T.E. (1988). Inorganic analogues of Langmuir-Blodgett films: Adsorption of ordered zirconium 1,10-decanebisphosphonate multilayers on silicon surfaces. *J. Am. Chem. Soc.* 110: 618–620.

59 Hanson, K., Torelli, D.A., Vannucci, A.K. et al. (2012). Self-assembled bilayer films of ruthenium(II)/polypyridyl complexes through layer-by-layer deposition on nanostructured metal oxides. *Angew. Chem. Int. Ed.* 51: 12782–12785.

60 Yoshimura, N., Kobayashi, A., Yoshida, M., and Kato, M. (2020). Enhancement of photocatalytic activity for hydrogen production by surface modification of Pt-TiO_2 nanoparticles with a double layer of photosensitizers. *Chem. Eur. J.* 26: 16939–16946.

61 Huang, J.F., Lei, Y., Luo, T., and Liu, J.M. (2020). Photocatalytic H_2 production from water by metal-free dye-sensitized TiO_2 semiconductors: the role and development process of organic sensitizers. *ChemSusChem* 13: 5863–5895.

62 Maeda, K., Sahara, G., Eguchi, M., and Ishitani, O. (2015). Hybrids of a ruthenium(II) polypyridyl complex and a metal oxide nanosheet for dye-sensitized hydrogen evolution with visible light: effects of the energy structure on photocatalytic activity. *ACS Catal.* 5: 1700–1707.

63 Maeda, K., Eguchi, M., Youngblood, W.J., and Mallouk, T.E. (2008). Niobium oxide nanoscrolls as building blocks for dye-sensitized hydrogen production from water under visible light irradiation. *Chem. Mater.* 20: 6770–6778.

64 Han, L., Lv, Y., Li, B. et al. (2020). Enhancing H_2 evolution and molecular oxygen activation via dye sensitized $BiOBr_{0.9}I_{0.1}$ under visible light. *J. Colloid Interface Sci.* 580: 1–10.

65 Zhang, W. and Lu, G. (2016). The enhancement of electron transportation and photo-catalytic activity for hydrogen generation by introducing spin-polarized current into dye-sensitized photo-catalyst. *Catal. Sci. Technol.* 6: 7693–7697.

66 Kong, C., Han, xia, Y., Hou, jie, L., and Li, ying, Y. (2017). Gathered sensitizer on the surface of catalyst by sodium polyacrylate for highly efficient photocatalytic hydrogen evolution. *J. Photochem. Photobiol. A Chem.* 345: 92–97.

67 Tajima, T., Yamagami, M., Sagawa, R. et al. (2021). Dye-sensitized H_2 evolution from water facilitated by photoinduced electron transfer between molecules on the inside and the outside of a carbon nanotube. *J. Appl. Phys.* 129: 014303.

68 Wu, L., Tong, Y., Gu, L. et al. (2018). MOFs as an electron-transfer-bridge between a dye photosensitizer and a low cost Ni_2P co-catalyst for increased photocatalytic H_2 generation. *Sustain. Energy Fuels* 2: 2502–2506.

69 Liu, X., Zhao, L., Wang, H. et al. (2018). Visible-light-driven H_2 production and decomposition of 4-nitrophenol over nickel phosphides. *RSC Adv.* 8: 34259–34265.

70 Lei, Q., Long, X., Chen, H. et al. (2019). Facilitating charge transfer *via* magnetoresistance effect for high-efficiency photocatalytic hydrogen production. *Chem. Commun.* 55: 14478–14481.

71 Panagiotopoulos, A., Douvas, A.M., Argitis, P., and Coutsolelos, A.G. (2016). Porphyrin-sensitized evolution of hydrogen using Dawson and Keplerate polyoxometalate photocatalysts. *ChemSusChem* 9: 3213–3219.

72 Sun, Y., Sun, Y., Meng, X. et al. (2019). Eosin Y-sensitized partially oxidized Ti_3C_2 MXene for photocatalytic hydrogen evolution. *Catal. Sci. Technol.* 9: 310–315.

73 Wang, X., Chen, L., Chong, S.Y. et al. (2018). Sulfone-containing covalent organic frameworks for photocatalytic hydrogen evolution from water. *Nat. Chem.* 10: 1180–1189.

74 Wan, S., Gándara, F., Asano, A. et al. (2011). Covalent organic frameworks with high charge carrier mobility. *Chem. Mater.* 23: 4094–4097.

75 Sprick, R.S., Bonillo, B., Clowes, R. et al. (2016). Visible-light-driven hydrogen evolution using planarized conjugated polymer photocatalysts. *Angew. Chem. Int. Ed.* 55: 1792–1796.

76 Vyas, V.S., Haase, F., Stegbauer, L. et al. (2015). A tunable azine covalent organic framework platform for visible light-induced hydrogen generation. *Nat. Commun.* 6: 8508.

77 Walsh, J.J., Bond, A.M., Forster, R.J., and Keyes, T.E. (2016). Hybrid polyoxometalate materials for photo(electro-) chemical applications. *Coord. Chem. Rev.* 306: 217–234.

78 Tachikawa, T., Fujitsuka, M., and Majima, T. (2007). Mechanistic insight into the TiO_2 photocatalytic reactions: design of new photocatalysts. *J. Phys. Chem. C* 111: 5259–5275.

79 Hiskia, A., Mylonas, A., and Papaconstantinou, E. (2001). Comparison of the photoredox properties of polyoxometallates and semiconducting particles. *Chem. Soc. Rev.* 30: 62–69.

80 Gao, J., Cao, S., Tay, Q. et al. (2013). Molecule-based water-oxidation catalysts (WOCs): Cluster-size-dependent dye-sensitized polyoxometalates for visible-light-driven O_2 evolution. *Sci. Rep.* 3: 1853.

81 Merki, D., Fierro, S., Vrubel, H., and Hu, X. (2011). Amorphous molybdenum sulfide films as catalysts for electrochemical hydrogen production in water. *Chem. Sci.* 2: 1262–1267.

82 Liu, X., Xue, Y., Lei, Y. et al. (2018). Cobalt-activated amorphous MoS_x nanodots grown in situ on natural attapulgite nanofibers for efficient visible-light-driven dye-sensitized H_2 evolution. *ACS Appl. Nano Mater.* 1: 6493–6501.

83 Kim, Y.I., Atherton, S.J., Brigham, E.S., and Mallouk, T.E. (1993). Sensitized layered metal oxide semiconductor particles for photochemical

hydrogen evolution from nonsacrificial electron donors. *J. Phys. Chem.* 97: 11802–11810.

84 Oshima, T., Nishioka, S., Kikuchi, Y. et al. (2020). An artificial Z-scheme constructed from dye-sensitized metal oxide nanosheets for visible light-driven overall water splitting. *J. Am. Chem. Soc.* 142: 8412–8420.

85 Saupe, G.B., Mallouk, T.E., Kim, W., and Schmehl, R.H. (1997). Visible light photolysis of hydrogen iodide using sensitized layered metal oxide semiconductors: The role of surface chemical modification in controlling back electron transfer reactions. *J. Phys. Chem. B* 101: 2508–2513.

86 Zhang, X., Luo, D., Zhang, W. et al. (2018). Inhibition of hydrogen and oxygen recombination over amide–functionalized graphene and the enhancement of photocatalytic hydrogen generation in dye–sensitized AF–RGO/Pt photocatalyst dispersion. *Appl. Catal. B Environ.* 232: 371–383.

87 Nishioka, S., Oshima, T., Hirai, S. et al. (2021). Excited carrier dynamics in a dye-sensitized niobate nanosheet photocatalyst for visible-light hydrogen evolution. *ACS Catal.* 11: 659–669.

88 Zhu, Y., Murali, S., Cai, W. et al. (2010). Graphene and graphene oxide: synthesis, properties, and applications. *Adv. Mater.* 22: 3906–3924.

89 Park, S. and Ruoff, R.S. (2009). Chemical methods for the production of graphenes. *Nat. Nanotechnol.* 4: 217–224.

90 Huang, J., Wu, Y., Wang, D. et al. (2015). Silicon phthalocyanine covalently functionalized N-doped ultrasmall reduced graphene oxide decorated with Pt nanoparticles for hydrogen evolution from water. *ACS Appl. Mater. Interfaces* 7: 3732–3741.

91 Huang, J., Wang, D., Yue, Z. et al. (2015). Ruthenium dye N749 covalently functionalized reduced graphene oxide: a novel photocatalyst for visible light H_2 evolution. *J. Phys. Chem. C* 119: 27892–27899.

92 Li, S., Tan, J., Jiang, Z. et al. (2020). MOF-derived bimetallic Fe-Ni-P nanotubes with tunable compositions for dye-sensitized photocatalytic H_2 and O_2 production. *Chem. Eng. J.* 384: 123354.

93 Shi, Y. and Zhang, B. (2016). Recent advances in transition metal phosphide nanomaterials: synthesis and applications in hydrogen evolution reaction. *Chem. Soc. Rev.* 45: 1529–1541.

94 Susner, M.A., Chyasnavichyus, M., McGuire, M.A. et al. (2017). Metal thio- and selenophosphates as multifunctional van der Waals layered materials. *Adv. Mater.* 29: 1602852.

95 Barua, M., Ayyub, M.M., Vishnoi, P. et al. (2019). Photochemical HER activity of layered metal phospho-sulfides and -selenides. *J. Mater. Chem. A* 7: 22500–22506.

96 Pan, J., Shao, X., Xu, X. et al. (2020). Organic dye molecules sensitization-enhanced photocatalytic water-splitting activity of MoS_2 from first-principles calculations. *J. Phys. Chem. C* 124: 6580–6587.

97 Youngblood, J.W., Lee, S.H.A., Kobayashi, Y. et al. (2009). Photoassisted overall water splitting in a visible light-absorbing dye-sensitized photoelectrochemical cell. *J. Am. Chem. Soc.* 131: 926–927.

98 Xu, P., Huang, T., Huang, J. et al. (2018). Dye-sensitized photoelectrochemical water oxidation through a buried junction. *Proc. Natl. Acad. Sci. U. S. A.* 115: 6946–6951.

99 Wang, D., Sampaio, R.N., Troian-Gautier, L. et al. (2019). Molecular photoelectrode for water oxidation inspired by photosystem II. *J. Am. Chem. Soc.* 141: 7926–7933.

100 Põldme, N., O'Reilly, L., Fletcher, I. et al. (2019). Photoelectrocatalytic H_2 evolution from integrated photocatalysts adsorbed on NiO. *Chem. Sci.* 10: 99–112.

101 Lyu, S., Massin, J., Pavone, M. et al. (2019). H_2-evolving dye-sensitized photocathode based on a ruthenium-diacetylide/cobaloxime supramolecular assembly. *ACS Appl. Energy Mater.* 2: 4971–4980.

102 Farnum, B.H., Wee, K.R., and Meyer, T.J. (2016). Self-assembled molecular p/n junctions for applications in dye-sensitized solar energy conversion. *Nat. Chem.* 8: 845–852.

103 Wang, D., Wang, Y., Brady, M.D. et al. (2019). A donor-chromophore-catalyst assembly for solar CO_2 reduction. *Chem. Sci.* 10: 4436–4444.

104 Kamata, R., Kumagai, H., Yamazaki, Y. et al. (2021). Durable photoelectrochemical CO_2 reduction with water oxidation using a visible-light driven molecular photocathode. *J. Mater. Chem. A* 9: 1517–1529.

105 Zhang, H., Li, S., Lu, R., and Yu, A. (2015). Time-resolved study on xanthene dye-sensitized carbon nitride photocatalytic systems. *ACS Appl. Mater. Interfaces* 7: 21868–21874.

106 Ma, H., Ma, W., Chen, J.F. et al. (2018). Quantifying visible-light-induced electron transfer properties of single dye-sensitized ZnO entity for water splitting. *J. Am. Chem. Soc.* 140: 5272–5279.

107 Nishioka, S., Yamazaki, Y., Okazaki, M. et al. (2019). Defect density-dependent electron injection from excited-state Ru(II) tris-diimine complexes into defect-controlled oxide semiconductors. *J. Phys. Chem. C* 123: 28310–28318.